

University of Tübingen
Faculty of Science
Department of Computer Science

Master Thesis Computer Science

Simulation-Based Inference of Soil Resistivity from Vertical Electrical Sounding

Markus Deppner

July 29, 2024

Supervisor

Guy Moss
Machine Learning in Science
University of Tübingen and
Tübingen AI Center

Reviewers

Prof. Dr. Jakob Macke
(Computer Science)
Machine Learning in Science
University of Tübingen and
Tübingen AI Center

Prof. Dr. Reinhard Drews
(Geo- and Environmental Sciences)
Geophysics and Glaciology
University of Tübingen

Deppner, Markus:

*Simulation-Based Inference of Soil Resistivity from Vertical
Electrical Sounding*

Master Thesis Computer Science

University of Tübingen

Thesis period: 01.03.2024 – 01.09.2024

Abstract

Investigations of the Earth's subsurface are commonly conducted using geoelectric methods. Within this field, Vertical Electrical Sounding (VES) plays a prominent role. Conventional deterministic inversions of VES data yield a single optimal result, which is typically not accompanied by uncertainty estimation. Furthermore, gradual transitions of soil types are not well captured by the inverted block model results. This work presents a probabilistic approach to inversion of VES data under a Schlumberger survey configuration. I utilize simulation-based inference (SBI), which is capable to provide uncertainty quantification, and allows incorporating spatially regularized smoothness into inferred soil transitions. Four models were trained under different prior distributions representing different soil characteristics. I tested the models against several synthetic instances of soil compositions with different characteristics, as well as to real measurements that were confirmed by a sediment core. Three models were able to match and even outperform state-of-the-art deterministic inversion results. As of now, there is no centralized nor standardized way of inverting measurements. With the aim to strive towards greater uniformity in geoelectric inversions, I developed a web application that deploys the trained SBI models. This application provides a centralized platform for inversion of VES data and potentially further geophysical inversion problems, as the field of geophysics offers great potential to apply this workflow to further methods.

Declaration

I hereby declare that I have written this thesis by my own, that I have not used any aids and sources other than those indicated and that I have marked all statements taken verbatim or in spirit from other works as such.

29.07.2024, Tübingen,



date, place, signature

Contents

1	Introduction	1
2	Methodology	6
2.1	Forward Model	6
2.1.1	1D Direct Current Resistivity Method	6
2.1.2	Noise Model	8
2.2	Inference	9
2.2.1	Simulation-Based Inference	10
2.2.2	Neural Posterior Estimation	10
2.2.3	Choice of Prior Distribution	12
2.3	Simulation-Based Coverage Calibration	15
3	Results	16
3.1	Synthetic Test Case	16
3.1.1	Data Generation and Evaluation	16
3.1.2	Inference Results	17
3.2	Evaluation on Drilling confirmed VES	21
3.2.1	Data	21
3.2.2	Inference Results	21
3.3	Simulation-Based Calibration	25
4	Discussion	27
4.1	Influences on Inference Uncertainties	27
4.2	Choice of Prior Distribution	29
4.3	Evaluation and Limitations of Models Performance	31
5	WebApplication - VESBI	33
5.1	Implementation Details	34
5.2	Outlook on additional Features	35
6	Conclusion	37

Chapter 1

Introduction

Knowledge about the subsurface is valuable for our understanding of the Earth and will benefit the sustainable use of its resources (Volchko et al., 2020; Van Ree and van Beukering, 2016). The subsurface is a multifunctional natural resource, which provides physical space, water, energy, materials, habitats for ecosystems, support for surface life, and a repository for cultural heritage and geological archives (Volchko et al., 2020). The first geophysical methods that measure the Earth's physical properties were developed over 100 years ago to investigate its subsurface structure (Best, 2015). Back then, the primary motivation behind such investigations was to locate mineral and petroleum deposits (Reynolds, 2011). Nowadays, these methods are applied in various fields, including environmental studies (McCarthy and Zachara, 1989), agriculture (Koganti et al., 2020), engineering (Chambers et al., 2006), archaeology (Appel et al., 1997) or hydrology (El Makrini et al., 2022; Abdullahi, 2015). Its applications range from finding suitable sites for new fountains or construction ground, to analyzing groundwater potential or archaeological sites remains.

Among the many techniques to investigate the subsurface, electrical resistivity surveys are one of the oldest and are still widely used today (Loke et al., 2013). The main advantages of geoelectrics are that it is quick to measure and does not require expensive equipment compared to other techniques such as seismic, magnetic or gravity (Loke et al., 2013). This method is applicable to a wide range of targets and is capable of investigating structures on a scale from millimeters to kilometers (Linderholm et al., 2008; Storz and Jacobs, 2001). Another notable advantage of the geoelectric method is its ability to create two-dimensional (2D) and three-dimensional (3D) profiles of the subsurface, compared to borehole drilling, which only yields data from single one-dimensional (1D) point measurement.

In the field of geoelectrical imaging, 2D imaging surveys are the most

widely, commercially applied technique, to obtain a 2D resistivity depth profile (Loke et al., 2013). This technique is based on electrical resistivity tomography (ERT) which uses multiple electrodes along a profile line to create a 2D resistivity depth profile. To validate the 2D profile, Vertical Electrical Sounding (VES), which is a 1D direct-current (DC) resistivity method, can be applied in addition to gather further information about specific locations (Zarroca et al., 2011). Instead of direct 2D profiling via ERT, which requires more equipment, quasi 2D profiles can be interpolated from multiple VES observations along a profile line. This is a low-cost method that is well suited for regions with technological or economic constraints (Riss et al., 2011). In this project, I am focusing on the 1D DC resistivity technique used for VES, due to its relevance in the field of geoelectric and its lower complexity compared to 2D or 3D imaging.

In VES, directed current is induced in the ground via two current electrodes A and B which generates a current flow and a potential field in the ground. The potential field is measured via the potential difference between the two potential electrodes M and N (Fig. 1.1). The current flow and the potential field is dependent on the electrode configuration, which is why multiple potential differences are measured with increasing AB distances. The observed potential differences can then be converted to the *apparent resistivity* signal, which is diagnostic to the true resistivity of the individual subsurface layers. However, obtaining the true resistivity distribution in the ground from the measured apparent resistivity signal can only be done through *inversion*.

Inversion also referred to as the *inverse problem* or *inference problem*, denotes the process of finding those parameters that are likely to cause our observation while being compatible with our prior knowledge. The inverse problem starts from the observation, for example the effect of a measuring technique, and derives the parameters underlying the observation, which is a ubiquitous problem in many areas of science and technology. Especially in the field of geosciences, where forward models are used to explain the effects of surveying techniques, inversion is a widespread problem (Snieder and Trampert, 1999) as for example in seismology (Russell and Hampson, 1991), hydrology (Zhou et al., 2014), oceanography (Roemmich, 1981), glaciology (Moss et al., 2023) or climate science (Lopez-Gomez et al., 2022; Pétron et al., 2002).

Over time, numerous methods have emerged for the inversion of VES data. Inman et al. (1973) introduced a generalized linear inverse theory, which was improved by using ridge regression (Inman, 1975) and later by least-squares (Hoversten et al., 1982; Lines and Treitel, 1984). New methods of inversion have been developed since then, which for example are based on singular value

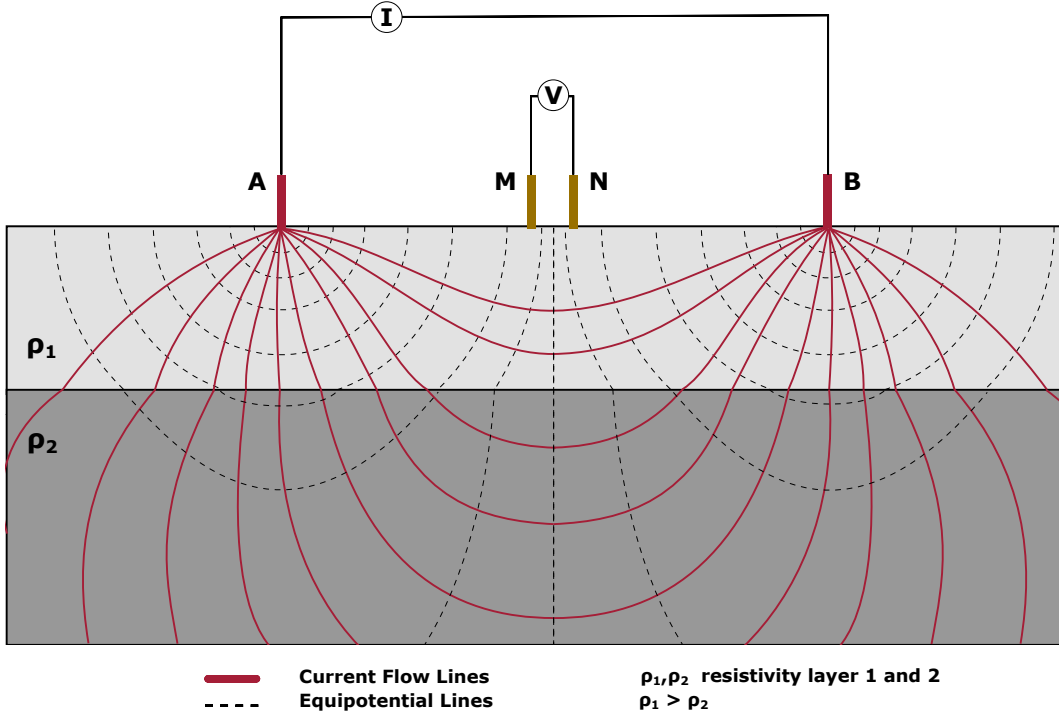


Figure 1.1: Experimental Setup of VES under Schlumberger electrode configuration. Current is injected into the ground via two current electrodes AB, which generates a current flow, indicated with red lines. The resulting potential field is indicated through dashed equipotential lines and is measured via the potential electrodes M and N. The potential difference between M and N is measured under varying AB distances.

decomposition (Heriyanto and Srigutomo, 2017), controlled random search (Bortolozo et al., 2015), or neural networks (El-Qady and Ushijima, 2001; Stephen et al., 2004). However, sequential least-squares inversion is still widely used nowadays in software applications such as SimPEG (Rücker et al., 2017) or pyGIMLi (Cockett et al., 2015). A common feature of existing inversion methods and frameworks is that, with a few exceptions (e.g. Piatti et al., 2010; Blatter et al., 2022), they typically do not provide information on the uncertainties of their inversion results. However, uncertainty quantification is valuable for the interpretation of the results, especially when additional information about the survey site is available. For instance, when data from other surveying techniques of the same site yield different results, uncertainty analysis can facilitate the integration and interpretation of these results.

Within this work, I investigate a probabilistic approach towards inversion of VES, which is able to provide uncertainty quantification with the inferred results. A typical probabilistic approach to the inversion problem is Bayesian Inference. Technically, the likelihood function is accessible through the deter-

ministic 1D DC resistivity forward model. However, Bayesian Inference is not well suited for deterministic likelihood-functions, as it can lead to posterior distribution degeneracy, and lacks robustness to model misspecification. To approximate Bayesian Inference, I employed a *likelihood-free* approach utilizing Simulation-Based Inference (SBI). This method evaluates simulations from a forward model under various parameters, sampled from a prior distribution (Cranmer et al., 2020; Papamakarios and Murray, 2018). Based on the simulations and its underlying model parameters, I train a neural network to obtain a conditional density estimation. In the case of Neural Posterior Estimation (NPE), which is the SBI variant chosen for our approach, the conditional density estimation from the network directly approximates the Bayesian posterior distribution (Papamakarios and Murray, 2018; Cranmer et al., 2020). A key advantage of NPE is that once the parameter samples are simulated and the network is trained, the conditional density estimation is amortized (Papamakarios and Murray, 2018; Greenberg et al., 2019). This means that the computationally expensive steps of simulation or training do not need to be repeated for unseen observations, and inference can be performed directly on the posterior network. Amortization of simulation cost is especially valuable as it opens the possibility to train the model once and provide the community access to the models. This allows users to obtain fast evaluation of measured apparent resistivities.

To take advantage of the amortization of NPE, I created a web application that hosts this novel approach and serves as a platform for fast geoelectric inversion. This application employs the pre-trained models, and provides a platform to infer soil resistivities from VES. At present, geoelectrical inversion tools are currently initialized and executed on an individual basis and in a manner that varies from one case to the next. This application has the potential to become a valuable tool to researchers, companies and institutions as the inversion process becomes centralized and standardized. With this platform, I want to take an active step in terms of science communication. Deploying the models on the platform and granting access to the geoelectric community, promotes the work that has been carried out in this project without the need to implement this workflow locally.

This project introduces a probabilistic approach to inverting data from VES using Neural Posterior Estimation. The aim of this work is to address limitations of deterministic inversion methods and enhance the inversion process, for example by providing uncertainty estimates. An exemplary workflow is demonstrated by training posterior networks under four different prior distribution and deploying them on the web application. As this workflow can be extended and transferred to other geophysical domains, the platform has potential to host a variety of inversion models, that are based on SBI, in the

future. This application provides a user-friendly platform for standardized inversion of geoelectric data. The study aims to lay the foundation for a web-based platform that goes beyond the geoelectric domain and extends to other geophysical inversion methods.

The thesis is structured as follows: In section 2, I present the methodology used in this project, starting with the description of the 1D DC resistivity forward model, followed by the description of the inference approach. In section 3, I show the models' performance on several synthetic test cases as well as real VES data, that is confirmed by a sediment core sample. The results will then be interpreted and discussed in section 4. Section 5 outlines the web application that hosts the models from this inversion approach. In the last section of this thesis, I summarize the work that has been carried out during this project. The code of the web-application and the analysis as well as the models and data will be available here: <https://u-017-s250.v263.uni-tuebingen.de/geophysics-tuebingen/research-projects/msc/2024-simulation-based-inference-of-soil-resistivities-from-ves>.

Chapter 2

Methodology

2.1 Forward Model

2.1.1 1D Direct Current Resistivity Method

Direct current resistivity methods refer to a group of geophysical techniques that induce directed current into the ground with the goal of assessing the subsurface structure arising from the varying resistivities of different soil types. The mechanisms of VES are represented by the DC resistivity forward model. The general procedure is to establish the current distribution in the subsurface and the potential field created along with it when inducing current into the ground ([McGillivray, 1992](#)) (Fig. 1.1). The aim of generating and measuring the potential field in the ground is to determine the spatial resistivity distribution of the subsurface ([Seidel and Lange, 2007](#), p.205).

Based on Ohm's law

$$\Delta U = RI, \quad (2.1)$$

conclusions about the resistivity R of the subsurface can be drawn, as the injected current I is known and the voltage difference ΔU can be measured. Assuming an isotropic conductive ground with conductivity σ , the flow pattern of the current density j and the electric field intensity E are described by the vectorized version of Ohm's law

$$\vec{j} = \sigma \vec{E} = -\sigma \nabla U, \quad (2.2)$$

which can be simplified to

$$\vec{E} = -\nabla U, \quad (2.3)$$

through the conservation of the stationary electrical field ([El-Qady and Ushijima, 2001](#)). The current density j is oriented along the direction of movement of charges and proportional to the electrical field strength, which is equivalent

to the electric potential gradient (Binley and Slater, 2020a, p. 22). Equation 2.3 states that the electrical field is equivalent to the negative derivative of the potential field and is therefore perpendicular to the equipotential lines of the electrical potential field. The generated potential at distance r from a point electrode that induces current into a homogeneous half-space with resistivity ρ is given by

$$U = \frac{I\rho}{2\pi r} \quad (2.4)$$

(Seidel and Lange, 2007, p. 207). For a single point electrode, the resistivity can then be expressed as

$$\rho = \frac{2\pi r U}{I}. \quad (2.5)$$

For a homogeneous and isotropic sub-surface, the derived resistivity would equal the true resistivity, but does not hold for a heterogeneous sub-surface. Therefore, this resistivity is referred to as the *apparent resistivity*, as it does not reflect the true resistivity of the subsurface layers, but is diagnostic to it.

The Vertical Electrical Sounding (VES) technique consists of measuring the variations in apparent resistivity ρ_a as a function of depth (El Makrini et al., 2022). A typical measurement setup for VES is the Schlumberger configuration where current is injected through the current electrodes A and B and the potential difference is measured via potential electrodes M and N located in between (Fig. 1.1). The depth of investigation in this setup is dependent on the distance between the current electrodes AB, where greater depth is reached through larger electrode distances. In a heterogeneous sub-surface, where several layers of varying thickness and resistivity are present, the apparent resistivity changes depending on the penetration depth of the electrical flow and the individual resistivity of the layers. The apparent resistivity becomes a function of the configuration of the electrodes, denoted in the configuration factor K

$$\rho_a = \frac{2\pi\Delta U}{I} K \quad (2.6)$$

which is defined as

$$K = \left(\frac{1}{AM} - \frac{1}{BM} - \frac{1}{AN} + \frac{1}{BN} \right)^{-1}. \quad (2.7)$$

The heterogeneous subsurface is represented as a sequence of individual layers with resistivity ρ_i and thickness d_i ($i = 1, 2, \dots, N$) where $i = 1$ represents the first upper layer. At the horizontal layer boundaries, the current flow is refracted and reflected according to the reflection coefficient

$$k_{i,i+1} = \frac{\rho_i - \rho_{i+1}}{\rho_i + \rho_{i+1}}. \quad (2.8)$$

For the assumption of multiple horizontal layers under a Schlumberger configuration, the apparent resistivity can be rewritten in an integral form that respects the layer thickness d_i , the reflection coefficients k and the electrode distance $\frac{AB}{2}$, here denoted as s . The analytical solution to the layered earth model

$$\rho_a = s^2 \int_0^\infty T_s(\lambda, k, d) J_1(\lambda s) d\lambda \quad (2.9)$$

composes of J_1 , which is the first order Bessel function of the electrode spacing s , λ as the integration variable and T_s is referred to as the *resistivity transform function* that is governed by the reflection coefficients and the thickness d (Binley and Slater, 2020b, p. 216). This integral of the analytical solution is commonly referred to as the *Hankel Transform* under the kernel T_s (Binley and Slater, 2020b, p. 216). With this solution, the apparent resistivity can be solved, given any layered subsurface and array configuration.

In this project, I used SimPEG's implementation of the 1D DC resistivity forward model. SimPEG is an open source framework for simulation and gradient based parameter estimation in geophysical applications (Cockett et al., 2015) and provides multiple python based implementations of geophysical forward models, and inversion methods. The measurement configuration of the forward model uses a logarithmic spacing of AB/2 electrode distances ranging from 2m to 100m under 23 measurement points. The distance between M and N is 2m. This electrode spacing is used by Terrana Geophysik for VES and was implemented in the forward model, with the aim to later validate the models on real data which was provided by Terrana Geophysik.

2.1.2 Noise Model

To account for measurement errors, noise was added to the simulations of the forward model. Incorporating noise is a common practice in machine learning, such as in computer vision using data augmentation (Shorten and Khoshgoftaar, 2019), speech recognition (Graves et al., 2013) or many other fields. Noise is a desired property to include in the training samples, as it often aids generalization and fault tolerance (Reed and Marks, 1999). Inference of noisy real world observations becomes more robust when trained initially on noisy data due to its benefit in generalization (Bishop, 1995). I include a white noise term $\varepsilon \sim \mathcal{U}_{[-5,5]}$, sampled randomly from a uniform distribution with magnitude $\pm 5\Omega m$, in the simulations to mimic real-world measurement errors. I have ascribed a rather minor role to the type of noise in this context; one could also have defined a Gaussian distribution or a stochastic process here. For the sake of simplicity, I have opted for a uniform distribution. I add a noise with magnitude of $\pm 5 \Omega m$ to each observation point of the simulated apparent

resistivity signal. This magnitude was chosen to maintain the integrity of the smooth and minimally fluctuating apparent resistivity signal, and to avoid distorting the signal by adding too much noise, especially for signals of low apparent resistivity.

2.2 Inference

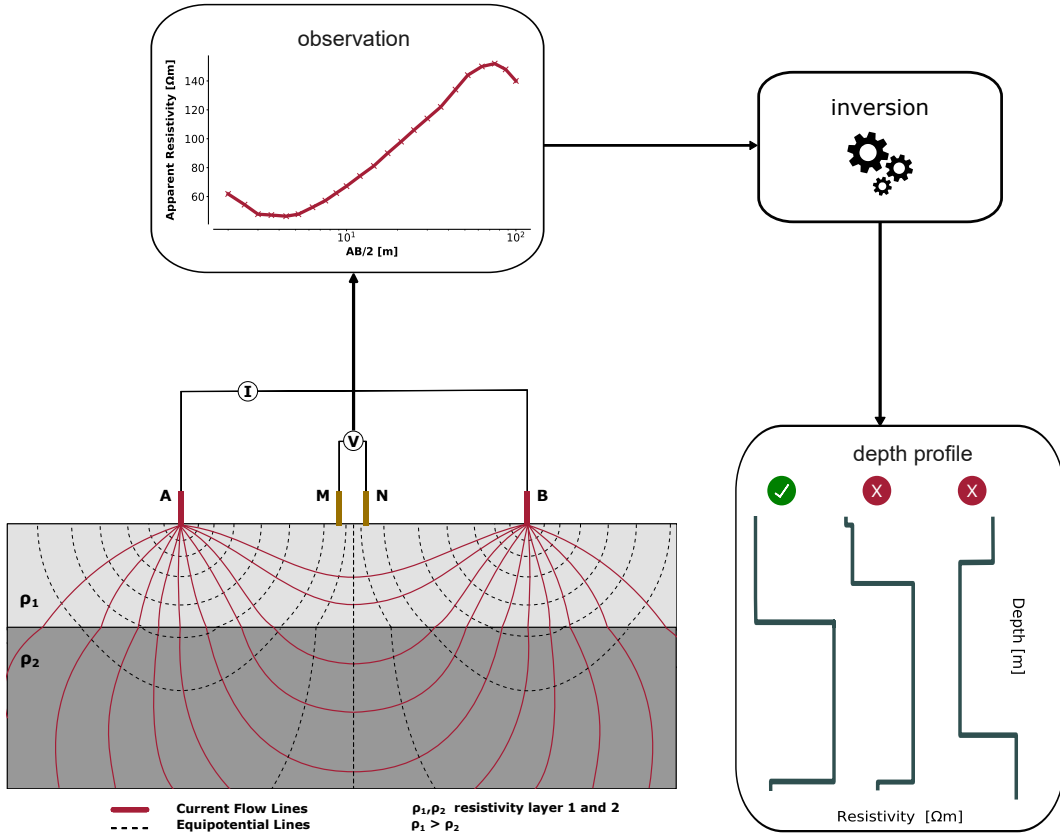


Figure 2.1: Schematic workflow of VES, and its inversion process to obtain the resistivity depth profile of a survey site. VES is conducted using the Schlumberger configuration with two current electrodes AB and two potential electrodes MN. Measured potential differences under varying AB electrode spacings yield the observed apparent soil resistivity signal. The resistivity depth profile that most likely caused the observation is inferred through inversion of the observed signal. Three inverted resistivity depth profiles are shown, where only the first matches the actual subsurface structure.

The focus shifts towards the *inverse problem*, as I ultimately want to determine those parameters θ that best explain the observation X given prior knowledge. The relationship between the sub-surface model parameters and

the observations is established by Bayes' theorem

$$p(\theta|X) = \frac{p(X|\theta)p(\theta)}{p(X)}. \quad (2.10)$$

As the evidence is intractable in many scenarios, and the likelihood-function is either ineligible, intractable, or originates from a deterministic forward model as in this case, methods evolved to approximate Bayesian Inference omitting these limitations. Likelihood-free inference or simulation-based inference address the problem of statistical inference without explicit access to the likelihood-function, or under unsuitable likelihood-functions, as in this deterministic case.

2.2.1 Simulation-Based Inference

SBI approximates conditional probability distributions based on samples from the forward model. This conditional probability distribution is approximated by using artificial neural networks which are trained, in order to approximate Bayesian inference (Fig. 2.2). Among different variants of SBI, where the conditional density function targets either the likelihood, the likelihood ratio, or the posterior distribution (see [Cranmer et al., 2020](#), for an overview), I opt for NPE which directly approximates the posterior distribution ([Greenberg et al., 2019](#)).

2.2.2 Neural Posterior Estimation

Neural Posterior Estimation uses conditional density estimation (CDE), to estimate the posterior density $p(\theta|X)$ from simulations X ([Greenberg et al., 2019](#)). The implementation in the SBI-toolkit([Tejero-Cantero et al., 2020](#)) utilizes normalizing flows to model the posterior distribution, which refers to the work of [Greenberg et al. \(2019\)](#). Normalizing flows transform simple base distributions (e.g. multivariate Gaussian) into complex distributions by a series of invertible and differentiable transformations f using neural networks with parametrization ϕ ([Durkan et al., 2019](#)).

A neural network F with weights ϕ is trained such that it learns the mapping from simulations X to the required transformations to best represent the posterior distribution. This is achieved by adjusting the network's weights ϕ , such that the network F approximate $q_{F(X,\phi)}(\theta) \approx p(\theta|X)$. The training dataset $\{(\theta_i, X_i)\}_{i=1}^N$ is composed by sampling parameters $\theta_i \sim p(\theta)$ from the prior distribution, and evaluation of the forward model to obtain the observation $X_i \sim p(X|\theta_i)$.

The network is then trained on the dataset to minimize the Kullback-Leibler (KL) divergence between the true posterior $p(\theta|X)$ and the approxi-

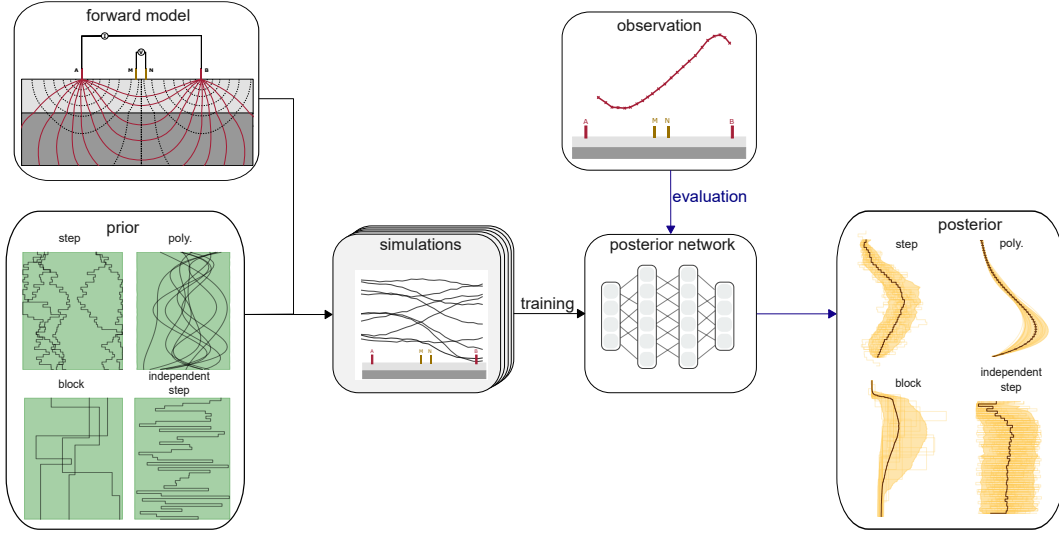


Figure 2.2: Simulation-based Inference workflow. Soil profiles are randomly sampled from one of the prior distributions, the corresponding apparent resistivity signal under respective AB/2 electrode configuration is obtained from the forward model. The neural network is trained on the simulations of the prior, which parameterizes conditional distributions. During the evaluation phase, the trained network is conditioned on the observed apparent resistivity and outputs the Bayesian posterior distribution over the parameters.

mated posterior $q(\theta|X, \phi)$

$$D_{KL}(p||q) = \int p(\theta|X) \log \left(\frac{p(\theta|X)}{q(\theta|X, \phi)} \right) dX. \quad (2.11)$$

From the KL divergence, it is possible to derive the loss function

$$\mathcal{L}(\phi) = - \sum_{i=1}^N \log q_{F(X_i, \phi)}(\theta_i), \quad (2.12)$$

or commonly denoted as

$$\mathcal{L}(\phi) = \mathbb{E}_{\theta \sim p(\theta), X \sim p(X|\theta)} [-\log q_\phi(\theta|X)], \quad (2.13)$$

on which the network is trained, by adjusting the parameters ϕ . Having established the loss function, the network can be trained, such that it finds the best parameters for the normalized flow that creates the posterior distribution given a set of simulations. Papamakarios and Murray (2018) has shown that under some assumption the minimum of this loss is reached when the estimated posterior matches the true posterior and $q_\phi(\theta|X) = p(\theta|X)$.

2.2.3 Choice of Prior Distribution

Tobler (1970) invoked the well cited first law of geography, which states that

“[...] everything is related to everything else, but near things are more related than distant things” (p. 236).

This empirical regularity is applicable beyond the geographical, regional and social sciences and motivated the choice of the following prior distributions. The prior represents the a priori understanding of the parameter distribution, which is usually opted by an expert of that domain. A well-chosen prior can improve efficiency, reduce uncertainty, and also incorporate domain knowledge into the model. At the same time, the prior distribution is a source of bias within the system. I trained four different posterior networks, each on simulations from a different prior distribution, with the aim of enforcing different qualitative properties on the material transitions (Fig.2.3). In deterministic inversion, layers are decoupled from each other, allowing large jumps in resistivity within small changes in depth. Although such structures are present in the subsurface, layer transitions without sharp layer boundaries, that show gradual transitions between soil layers are present as well, for example when a sandy layer transitions to a gravel layer. I aimed to incorporate smooth resistivity transitions in depth with the use of Legendre Polynomials and a spatially regularized step function as a prior to better account for such transitions. With the choice of those priors, I enforce learning smooth transitions, which is non-trivial to include in the deterministic inversion process. To address distinct layer changes, an independent step prior as well as a four layer block model was used as a prior distribution to train two further models. Each of the prior distributions are presented in the following subsections. The resulting models, trained on the respective prior distribution, are hereinafter referred to as the **step model**, **polynomial model**, **independent step model** and **block model**.

Spatially Regularized Step Prior

With the goal to incorporate smooth transitions in the depth profile, a spatially regularized prior, similar to a random walk prior, has been employed. The depth profile is represented in small discrete layers with fixed layer thickness of 0.5 meters, which reach a depth of 24 meters. This results in a total of 48 parameters. The resistivity value of the first layer θ_{r_0} is sampled from a uniform distribution $\mathcal{U}_{[1,1000]}$. To restrict the parameter space of the priors, I limited the maximal resistivity value to 1000 Ωm . Although there are soil types that exceed this range (Binley and Slater, 2020a; Reynolds, 2011), I had to compromise between the applicability of the models, in terms of maximal

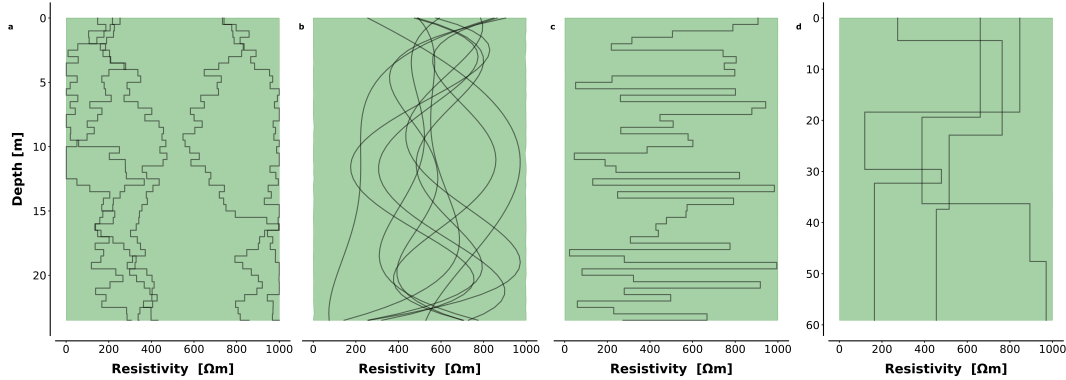


Figure 2.3: Samples from the four prior distributions used for training different posterior networks. Subplot **a** shows samples from the spatially regularized step prior **b** from the Legendre Polynomial prior **c** a single prior sample from the independent step prior and **d** from the four layer block model. The green shaded area is the covered space of 100,000 prior samples.

inferred resistivity values, and the required simulation and training costs. A larger parameter space requires the execution of a greater number of simulations to ensure the coverage of the entire space.

The following layer resistivity are spatially regularized s.t. the resistivity value is dependent on the resistivity of the previous layer, avoiding large resistivity jumps within small depth changes. The resistivity value of the i -th layer $\theta_{r_i} \sim \mathcal{N}(\theta_{r_{i-1}}, 50 \Omega m)$ is sampled from a normal distribution with mean $\mu = \theta_{r_{i-1}}$ and variance $\sigma^2 = 50 \Omega m$. This is equivalent to Brownian Motion or a Gaussian Process prior with a constant mean function $\mu_t = \mu(\theta_{r_0})$ which relates to the mean of the uniform distribution of the first layer, and kernel $\kappa(\theta_{r_i}, \theta_{r_j}) = \min(i, j)$. The kernel defines that layer resistivities at greater depth are only dependent on the previous layers, but not vice versa. To prevent the resistivities from exceeding or falling below our previously set value range, these values are clipped, which differs from a standard Wiener process. This definition incorporates smooth transitions within the subsurface, enforcing spatially close layers to be dependent on each other, and resistivity values of layers far apart to be less correlated.

Polynomial prior

The second approach to represent smooth layer transitions in the prior distribution was motivated to maintain smoothness while reducing parameter dimensionality. I choose to represent the sub-surface depth profile by a combination of the first five Legendre-Polynomials. Coefficients for the individual polynomials are sampled from a uniform prior distribution $c_i \sim \mathcal{U}_{[-1,1]}$. As

the polynomials are well-defined within the interval of $[-1, 1]$, the joint polynomials are scaled towards the defined resistivity space of $[1 - 1000 \Omega m]$. To avoid a distortion in the distribution of the prior space, and to maintain the integrity of the interval of $[-1, 1]$, I decided to discard coefficient combinations that would result in a polynomial that exceeds this interval. Given the nature of Legendre Polynomials, a combination of multiple polynomials can overshoot this range, especially towards the boundaries of the interval, which I avoided by invalidating such samples. As the forward model is not capable of handling continuous inputs, I evaluate the Legendre Polynomial at small discrete steps of 0.5m of depth, which results in 48 small layers as in the spatially regularized step prior. Through the nature of Legendre Polynomials, smoothness was incorporated while reducing the prior parameter space from a dimensionality of 48 to five.

Spatially Independent Step Prior

To address distinct layer jumps, another step prior was defined without spatial regularization. Again, small layers of magnitude 0.5m were defined up to a total depth of 24m, which are directly forwarded to the simulator. Individual resistivity values are sampled from the same uniform distribution $\mathcal{U}_{[1,1000]}$ as in the regularized step prior. Removing this spatial constraint increases the sample space drastically. This prior distribution, highly varying depth profiles with high resolution. It is the less restrictive prior and yields the highest degree of freedom in representing the depth profiles.

Four Layer Block Prior

The second prior composes a depth profile from four independent layers of varying depth. This prior is capable of inferring different depths along with the resistivities. It samples four resistivity values from a uniform distribution $\mathcal{U}_{[1,1000]}$, each of which represents one layer. Three further thickness values are sampled from another uniform distribution $\mathcal{U}_{[0.1,20]}$ that represent the magnitude of the layers. The last layer is assumed to reach to infinity, which holds for all prior distributions, which comes from the inherent representation in the forward model. This results in a total of seven parameters for that prior distribution. This is a rather general prior that despite the upper and lower limits of the resistivity values and layer thicknesses does not comprise any additional domain knowledge.

2.3 Simulation-Based Coverage Calibration

In order for the estimated posterior $q_\phi(\theta|x_o)$ to converge towards the true posterior $p(\theta|x_o)$, the estimated posterior needs to be broader than the true posterior distribution (Deistler et al., 2022; Rozet and Fin, 2021). The motivation here is to validate if the estimated posterior is sufficiently broad on average. Therefore, expected coverage tests, as proposed by (Deistler et al., 2022) which builds on the work of Dalmasso et al. (2020); Miller et al. (2021) and Hermans et al. (2022), are applied to check the conditional density estimators. The coverage of the approximate posterior can be computed as

$$1 - \alpha = \int q_\phi(\theta|x^*) \mathbb{1}(q_\phi(\theta^*|x^*) \geq q_\phi(\theta|x^*)) d\theta \quad (2.14)$$

where θ^* denotes samples from the estimated posterior as proposal and x^* is the corresponding simulator output. The expected coverage can be computed as an average of the coverage across multiple pairs (θ^*, x^*) (Miller et al., 2021; Hermans et al., 2021), and should match the confidence level for all confidence levels $(1 - \alpha) \in [0,1]$.

A valid SBC check is no guarantee that the posterior estimation is correct, but a failed check shows that the inference is unbalanced. SBC provides insights of whether the estimated posterior distribution is balanced, over-confident or under-confident.

Chapter 3

Results

A summary of the main findings, is provided in the following chapter. Prior to applying the models to actual measurements, their applicability is demonstrated using synthetic data, where the ground truth is known. Subsequently, the models infer the resistivity depth profile of a site, where VES is confirmed by a sediment core sample.

3.1 Synthetic Test Case

3.1.1 Data Generation and Evaluation

With this analysis, I want to evaluate the performance and sanity of the models and validate the approach taken in this study. I compare the probabilistic models that were trained on different prior distributions against each other to assess the characteristics and the suitability of the prior and the corresponding posterior distributions. Furthermore, I compare the models with three external state-of-the-art deterministic inversion models.

To make this comparison, I test all models, both probabilistic and deterministic, against several ground truths (GTs) that entail different soil characteristics in their depth profile. For this, I took ten random depth profiles sampled from each of the four prior distributions as they were introduced in section 2.2.3. These 40 samples represent the GTs in parameter space. The prior samples are evaluated under the forward model and the corresponding apparent resistivity signals serve as the GT in observation space.

Classical deterministic inversion methods minimize over the error of the apparent resistivity signal and derive the parameters of the depth profile from the best fit to the observed signal. To ensure a fair comparison between probabilistic and deterministic models, I consider those posterior predictive samples that best match the apparent resistivity signal. For each GT sample, I take

1,000 random posterior samples and evaluate them under the forward model. Among the 1,000 posterior predictive samples, I consider the one that yields the minimum root mean square error (RMSE) to be the best fit. Along with the best fitting posterior predictive sample, the depth profile underlying that prediction in parameter space is identified. This depth profile is compared to the GT depth profile and the RMSE between them is calculated. For each of the prior distributions, the minimum RMSEs of the model are averaged over the ten prior samples. This demonstrates the model’s performance under samples originating from that prior distribution.

To compare the probabilistic models with the deterministic inversion methods, I inverted the synthetic GTs under three deterministic models that assume different numbers of layers. To match the layer assumptions in our probabilistic models, I chose a four-layer deterministic model and a 48-layer model. For the performance on real VES observations, I also considered a five-layer model, as the sediment core can be grouped into five layers. As the deterministic models yield only one single result, the RMSE of that result is computed in observation and parameter space. For each of the prior distributions, I calculate the average of all RMSE values over the ten GT samples from a given prior distribution.

3.1.2 Inference Results

The error metrics in observation space are shown in Table 3.1 and the RMSEs in parameter space in Table 3.2. A single representative GT sample from the step prior and the inference results of all inversion models are presented in Fig. 3.1 (see Fig. 6.1 for a GT sample from the polynomial prior and Fig. 6.2 for a GT sample from the block prior).

According to the average error metrics in observation space, the probabilistic models perform best when the GT is from the same prior distribution as the one on which they were trained. A visual comparison of the models’ inference results demonstrates different behavior in their inferred depth profiles, strongly reflecting the characteristics of the prior. This shows that the different properties of the soil and its layer transitions, which were incorporated by the prior distribution, were also transferred to the posterior distribution. This approach successfully incorporates additional prior knowledge about soil transitions and characteristics into the inference process, which is not possible in deterministic inversion methods. Since the posterior distributions reflects the prior distribution, it explains that the models perform best on GT samples from the same prior distribution they were trained on, as those samples share similar characteristics.

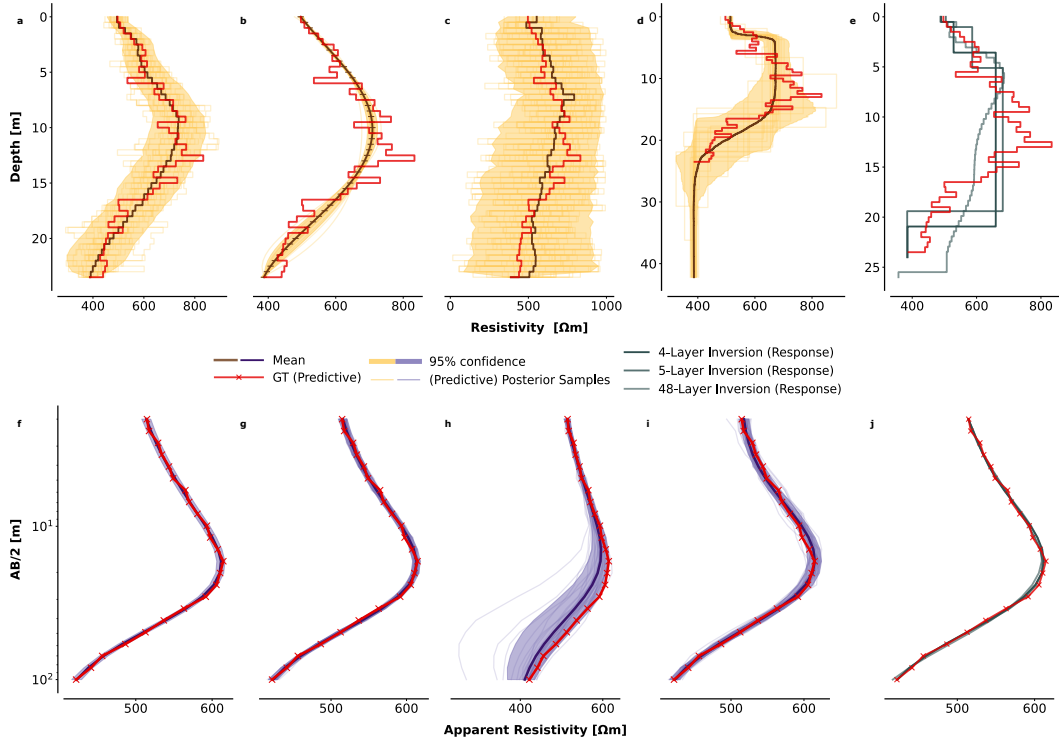


Figure 3.1: Posterior (Predictive) for a single synthetic ground truth sample from spatially regularized step prior. Subplots a - e show the depth resistivity profile in parameter space, f-j show apparent resistivity against $AB/2$ electrode spacing in observation space. a shows the model posterior network trained on the regularized step prior, b on the polynomial prior, c on the independent step prior d on the block prior. The respective posterior predictive of the models are showcased below. Subplots e and j show inversion and response of classic deterministic inversion of four, five and 48 layers.

The model trained on the spatially independent step prior shows the highest uncertainty among test instances, and also yields the highest error metrics of all models. Although this model was trained on 500,000 simulations (five times more than the other models) it is less confident in its predictions. Given the prior distribution, which has the highest degree of freedom, the posterior should in general be able to infer the GT samples, however it struggles in terms of accuracy. The errors are relatively high compared to the other models, except for samples from its own prior distribution. This problem can be traced back to the large parameter space that comes from removing the spatial constraint compared to the spatially regularized step prior. To improve its inference result, this model might need further training or a reduction of the parameter space.

Table 3.1: Average RMSEs in observation space of probabilistic and deterministic models tested against synthetic ground truths. RMSEs of the models reflect the average over all GT samples originating from the respective prior distribution, indicated with prior. The deterministic inversion results indicated with an *. The values here represent the \pm error relative to the GT in Ω_m .

	Step Model	Poly Model	Block Model	Ind. Step Model	4 Layer Det. Model	5 Layer Det. Model	48 Layer Det. Model
Step _{prior}	± 2.30	± 5.65	± 3.76	± 8.45	$\pm 5.77^*$	$\pm 3.76^*$	$\pm 3.92^*$
Poly _{prior}	± 2.84	± 2.53	± 3.65	± 7.98	$\pm 5.22^*$	$\pm 3.34^*$	$\pm 4.47^*$
Block _{prior}	± 5.85	± 3.51	± 2.49	± 6.33	$\pm 4.56^*$	$\pm 3.78^*$	$\pm 4.31^*$
Ind. Step _{prior}	± 4.06	± 6.87	± 7.46	± 3.19	$\pm 6.80^*$	$\pm 4.85^*$	$\pm 4.94^*$
Avg. All _{priors}	± 3.76	± 4.64	± 4.34	± 6.49	$\pm 5.59^*$	$\pm 3.93^*$	$\pm 4.41^*$

Table 3.2: Average RMSEs in parameter space of probabilistic and deterministic models tested against synthetic ground truths. RMSEs of the models reflect the average over all GT samples originating from the respective prior distribution, indicated with prior. The deterministic inversion results indicated with an *. The values here represent the \pm error relative to the GT in Ω_m .

	Step Model	Poly Model	Block Model	Ind. Step Model	4 Layer Det. Model	5 Layer Det. Model	48 Layer Det. Model
Step _{prior}	± 81.00	± 352.84	± 89.02	± 223.77	$\pm 104.82^*$	$\pm 101.96^*$	$\pm 84.88^*$
Poly _{prior}	± 83.45	± 11.36	± 123.59	± 272.08	$\pm 103.16^*$	$\pm 118.21^*$	$\pm 113.50^*$
Block _{prior}	± 152.69	± 123.79	± 77.59	± 286.39	$\pm 93.53^*$	$\pm 139.69^*$	$\pm 118.74^*$
Ind. Step _{prior}	± 345.07	± 338.20	± 335.07	± 353.29	$\pm 320.49^*$	$\pm 324.76^*$	$\pm 331.43^*$

Regarding the deterministic models, the results align with the hypothesis that a high degree of freedom does not necessarily enhance the models' performance. The 48-layer deterministic model has higher total average RMSE ($\pm 4.41 \Omega m$) than the five-layer model ($\pm 3.93 \Omega m$) and also on all individual priors. This underlines the importance of the parametrization of the depth profile when choosing an inference model or a suitable prior distribution. However, this model is still superior to the deterministic four-layer model in terms of average RMSEs on the test instances.

A comparison of the two four-layer models with each other shows that the probabilistic four-layer model outperforms the deterministic four-layer model on average over all GT samples of all prior distributions, with a mean RMSE of $\pm 4.34 \Omega m$ to $\pm 5.59 \Omega m$. The block model is among the models that yield the lowest errors on GT samples from the step, polynomial and block prior distribution. Within that GT samples, it outperforms the deterministic four-layer and also the 48-layer model. On the aforementioned GT samples, the probabilistic block model is able to yield posterior prediction samples that are as accurate, or even more accurate, than the inversion results of the deterministic five-layer model. These findings are also represented in the errors in parameter space (again excluding the independent step GTs), as the errors of the block model are in the similar magnitude as the deterministic inversions, or even lower. Although the block model yields the highest error on samples of the independent step prior ($\pm 7.46 \Omega m$), it is the model with the third-lowest average RMSE across all test instance. The block model is also able to provide good posterior predictive samples for the smooth GT samples from the regularized step prior and the polynomial prior. The block model has only a small number of layers, however it is the only probabilistic model that is able to infer the depth, which seems to be beneficial for the inference results.

The depth profile of the polynomial model has a fixed depth of 24m, and is represented by Legendre Polynomials, which only requires five parameters to represent a depth profile. The model yields high accuracy on GT samples from the block prior and its own polynomial prior, and generally shows small uncertainties in its inference results. Especially in comparison with the uncertainties of the smooth step model, the polynomial model seems to be more confident in its predictions. This may be due to the small parameter space of the prior distribution.

In general, the probabilistic models demonstrate superior performance compared to their deterministic counterparts, as there is always a model which leads to a better fit than the deterministic models.

3.2 Evaluation on Drilling confirmed VES

3.2.1 Data

The analysis on real measurements is based on internal and confidential data of the company Terrana Geophysik, Zeppelinstraße 15, 72116 Mössingen. They provided me data of vertical electrical soundings that are confirmed by a sediment core to evaluate the models' performance. Names, customer and sediment core numbers cannot be published, but the data is provided anonymously to ensure reproducibility of the results. There are no direct resistivity values associated with the core sample, but the ranges of resistivity of the materials are provided based on literature and experience values of Terrana Geophysik. The sediment core is only approximately 4 meters apart from the VES survey site.

3.2.2 Inference Results

The drilling core itself shows higher resolution layers, that were grouped into five main layers by Terrana. Two small top layers of silt/sand and silty sandy gravel reach together to a depth of 3.4m. Two layers of greater magnitude follow, where the composition of gravel, sand and silt changes. The last layer of silt terminates at a depth of 20.7m and shows low resistivity values between 10-70 Ωm (Fig 3.2).

The mean of the posterior samples from the step model (step model mean) starts with values of 100 Ωm for the first 1.5m, with consecutive layers up to 5m around a resistivity of 150 Ωm . These inferred values fall into the supported range of the soil resistivity values of the drilling core for the first two layers. The third layer, composed of sand, reaches until a total depth of 10m. The step model mean transitions between 5m and 10m from 150 Ωm to 500 Ωm , which exceeds the soil resistivity range of the sand layer. Between 10m and 15m, the step model mean is relatively consistent between 400 Ωm and 450 Ωm , which matches the fourth layer of gravel. After 15m of depth the inferred resistivity transitions to lower values, reaching a final value of 200 Ωm which is above the range of silt.

The mean of the posterior samples from the polynomial model (polynomial model mean) is rather constant in the first 5m in a magnitude of 200 Ωm and transitions into higher resistivity values after 5m of depth. The polynomial model mean transitions continuously towards a maximum resistivity value of 600 Ωm at a depth of 17m, which also exceeds the resistivity range of gravel. After the maximal resistivity at a depth of 17m, the mean transitions again to lower resistivity values, also terminating at a value of 200 Ωm . Despite the initial steady 5m that can be mapped to the first two layers, there is almost no

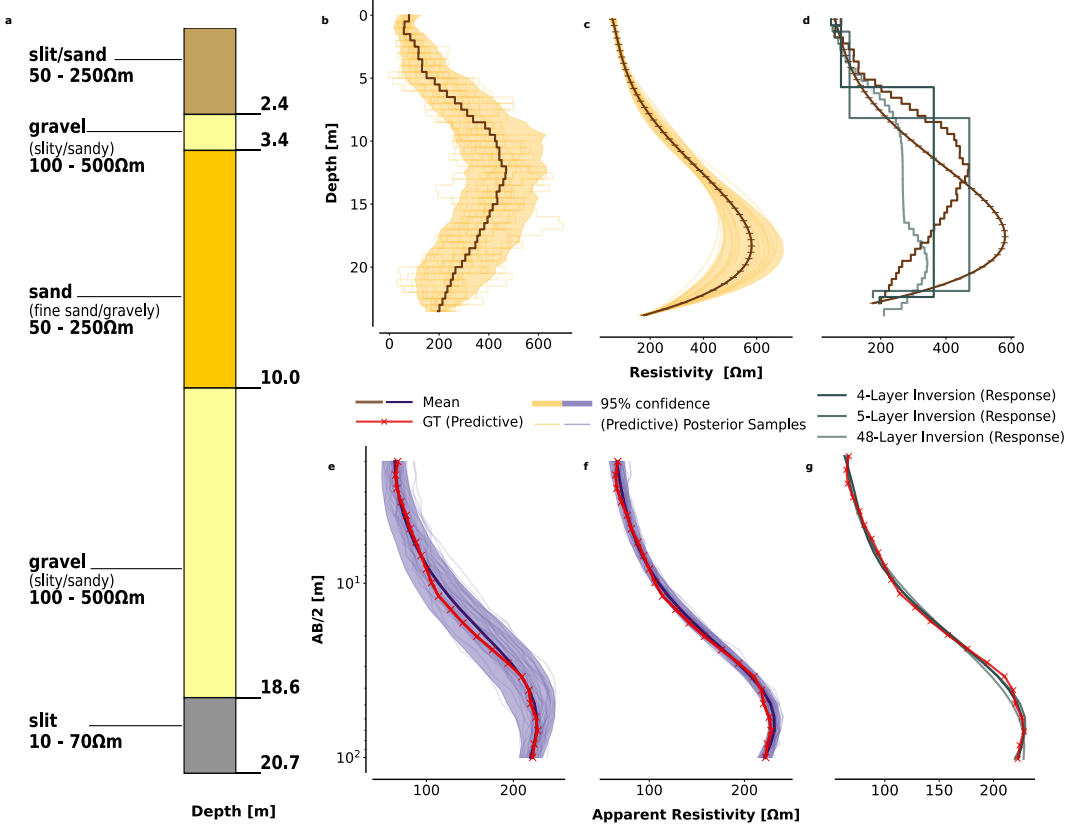


Figure 3.2: Inference results of step model and polynomial model on real VES data, that is confirmed by sediment core. Subplot a represents the sediment core that has been grouped into five layers by Terrana Geophysik. Subplot b and c show the posterior distribution of the step and polynomial model. The posterior predictive distribution is shown below in e, while f, d and f show the results of the deterministic inversion models.

similarity in the depth profile of the polynomial model mean to the sediment core. However, the predictive mean matches the signal with higher accuracy than the step model.

The deterministic inversion responses match the observed signal, but yield different layer transitions than present in the sediment sample. The four layer inversion has an initial small layer similar to the step model and another layer jump at a depth of 5m to a layer of higher resistivity, which has a magnitude of 15m and reaches to a total depth of 22m. All models converge to a final layer of around $200 \Omega\text{m}$. The 48-layer inversion shows a similar depth profile in the first 5m as the step model in the beginning, but has much lower resistivity layers between 5m and 20m than all other inversion results. This depth profile is quite different to the other results, as it does not reach re-

Table 3.3: Minimal and Average RMSEs in observation space of probabilistic and deterministic models tested against real observation. The minimum RMSE of 1,000 posterior predictive samples and the average RMSE across all samples is shown. The values here represent the \pm error relative to the GT in Ωm and the deterministic inversion results are indicated with a *. As the deterministic models only yield single results for a given observation, the average RMSE values cannot be computed and are therefore indicated with a - in the table.

	Step Model	Poly Model	Block Model	Ind. Step Model	4 Layer Det. Model	5 Layer Det. Model	48 Layer Det. Model
Min. RMSE	± 2.77	± 2.97	± 3.45	± 2.68	$\pm 3.00^*$	$\pm 2.41^*$	$\pm 4.83^*$
Avg. RMSE	± 14.80	± 5.43	± 6.22	± 36.63	-	-	-

sistivity values above 400 Ωm for any layer. It is also the model that yields the highest RMSE of all. A large number of layers might not be beneficial for deterministic inversion. The best result is yielded by the five-layer deterministic model, which assumes the right number of layers, although its inferred depth profile does not match with the layer boundaries in the sediment sample.

The block model yields accurate posterior predictive samples on average, but a relatively high RMSE on its single best posterior predictive sample. Despite large uncertainties in parameter space, originating from its variability in depth, the confidence intervals in observation space are as narrow as in the polynomial model (Fig. 6.3). The mean of the posterior samples from the block model (block model mean) shares similarities in transitions with the step model mean. Despite a wrong assumption of layers in this model, it yields robust and accurate inference results.

The independent step model has the highest uncertainties in its predictions, but is still capable to yield single good posterior predictive samples with high accuracy. Yet, the mean of its posterior samples, shows no similarities to the sediment sample and mostly assumes layers of 500 Ωm . The posterior predictive mean of that model is higher than the actual observation, and the mean RMSE is with great margin the highest. Nevertheless, the observation falls within the confidence interval of the posterior predictions. Despite difficulties in terms of accuracy, the model is still capable of inferring the observation.

The analysis of the real measurement confirm the results previously obtained from the analysis of synthetic data. The independent step model ac-

counts for the highest uncertainty in its predictions, but is still capable to provide single good posterior predictions. A more robust model is the block model that shows similarities with the sediment core in its depth profile and yields accurate average predictions. The polynomial model yields the lowest uncertainties and fits the observed signal well, with its single best posterior predictive sample and also on average. Despite showing the best results, the depth profile is not consistent with the provided sediment sample. The step model mean does show similarities with the sediment core, but this is not reflected in its average performance. This model has larger average RMSEs and higher uncertainties than the polynomial and block model, but is still capable of providing single posterior predictions with high accuracy. On this observation, the five-layer deterministic model yields the single lowest RMSE, but the probabilistic models are capable of providing more accurate results than the other two deterministic models.

Despite visually very different resistivity depth profiles showing great variety in their behavior and layer transitions, the probabilistic models are all capable of capturing the signal accurately with their best inversion results. However, they show very different resistivity depth distributions that might not match the depth profile of the sediment core.

3.3 Simulation-Based Calibration

To ensure that the estimated posterior $q_\phi(\theta|x_o)$ converges towards the true posterior $p(\theta|x_o)$, it must be broader than the true distribution. In addition to posterior predictive checks, I use expected coverage tests to validate the estimated posterior distributions. These tests show whether the posterior estimation is balanced, over-confident, or under-confident, which gives insights into the accuracy of the inference.

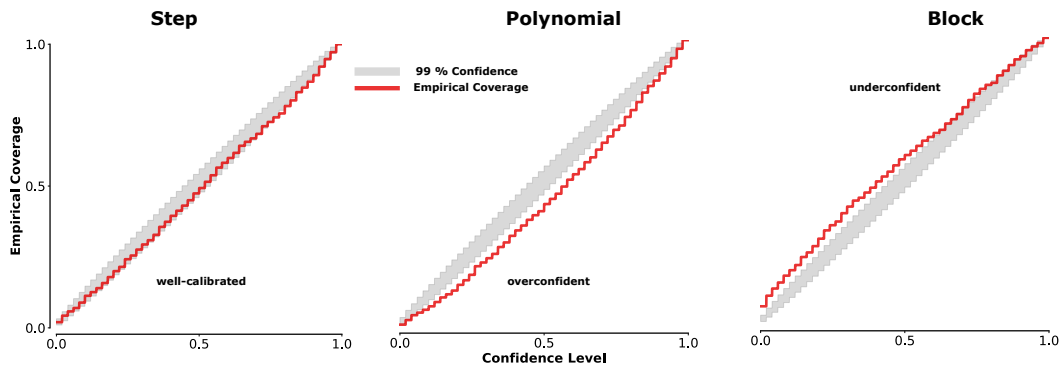


Figure 3.3: **Simulation-based Calibration of the expected coverage of the step model, polynomial model and block model.** The gray shaded area represents the 99% confidence interval of a uniform distributed coverage. The red line is the empirical coverage of the models under varying confidence intervals. The models were calibrated for 1,000 simulations, each of which utilized 1,000 posterior samples. A well calibrated model lies within the support of the uniform distribution. Empirical coverage below the shaded areas represent over-confidence and underconfidence above the shaded area (Deistler et al., 2022).

The step model shows good expected coverage that is right in the 99% confidence interval with no indication of invalid inference or miscalibration in the posterior distribution. However, the block model is above the 99 % confidence interval, indicating that the model is under-confident, which is consistent with the uncertainty estimates seen in the previous results. The under-confidence of the model can be traced back to multiple reasons. There is high variability in the data provided, as simulations vary in depth. The variability in depth is reason for a more complex likelihood-function of individual parameters, which is harder to learn and might require more simulations. Another explanation of this under-confidence is the degeneracy of the forward simulations. Especially under varying depths in the depth profile, a large variety of depth profiles are able to generate the same apparent resistivity signal, which makes it challenging to be certain about individual parameters. The uncertainty can be reduced to some extent by training on more simulations, however the parameter uncertainty due to the degeneracy of the forward model cannot be eliminated.

The polynomial on the other hand yields lower expected coverage across all confidence levels, indicating overconfidence in the model. This is also consistent with the findings throughout the conducted performance analysis, as the polynomial model generally has very narrow uncertainty bands. This can be attributed to the prior distribution, which might be too restrictive. The priors for the individual parameters might be too narrow and do not allow for sufficient variability in the samples. To describe a depth profile with the polynomial prior, the coefficients of the first five Legendre Polynomials are sampled. The combination of the individual Polynomials with respect to the coefficients compose the depth profile. Single polynomials are well-defined within the interval of [-1, 1], which might be exceeded for the combination of multiple polynomials. To maintain an equal distribution within this interval, I restricted the combination of multiple polynomials that exceed this interval. In terms of simulation efficiency, many combinations of coefficients exceed that limit and are handled as invalid. The over-confidence of the model might come from this restriction in parameter space, as the resulting variability in the samples might be too low. To address the overconfidence of the polynomial model, a broader parameter space needs to be allowed, while maintaining the equal distribution of trajectories within the resulting depth profiles.

The empirical coverage of the independent step model could not be computed due to the long runtime of the calibration on that model. The model has difficulties finding parameters on many observations, indicating that only a small amount of posterior samples are within the supported range of the proposal. This made sampling from the posterior extremely slow and the calibration check of the expected coverage infeasible on this posterior. A calibration on the single dimension ranks faced similar difficulties, but was feasible for 1,000 simulations and 500 posterior samples. The individual posterior ranks of that model are shown in Fig. 6.4. The posterior is not-well calibrated, as most cumulative distribution functions of the parameters are above the confidence interval for low ranks and below for higher ranks. This indicates that the posterior is skewed in both directions and has difficulties in accurately predicting parameters. This is consistent with the large uncertainties that the model showed within the analysis. To better calibrate the posteriors, the conditional density estimator needs to be trained on additional simulations.

Chapter 4

Discussion

The findings of this study demonstrate that a probabilistic approach to inversion of VES is feasible. It has the potential to enhance the inversion process of VES data by providing uncertainty quantification, but also with respect to performance and accuracy of the inversion results. The probabilistic models are able to meet or even outperform deterministic inversion models in terms of accuracy of their posterior predictive samples compared to the observed signal. However, the models' performance depend strongly on the simulations and therefore on the prior distributions they were trained and tested on. To address these points, I structured this section into three parts, starting with the discussion on the uncertainties, followed by the choice and the impact of the prior distribution on the inference process. In the last section, I discuss the performance of the models under the test instances and address the non-uniqueness of the forward model.

4.1 Influences on Inference Uncertainties

The inference results show that in the first few meters of the depth profile generally lower uncertainties are present compared to deeper layers. This is attributable to the measurement technique, as small AB electrode distances only penetrate the uppermost layers of the soil. At very small electrode distances, the measured apparent resistivity is approximately the true resistivity. With increasing AB distances, the signal is composed of multiple layers and their resistivity values in the subsurface. Individual small layers are superimposed by the magnitude of surrounding layers, which is why the uncertainty becomes greater with greater depth. However, the last layers show lower uncertainty again. The forward model assumes the last layer as an infinite homogeneous half space. At higher AB distances, this last layer is increasingly penetrated by the induced current, which lowers the uncertainty of its resistivity value. These effects have an influence on the uncertainties of the model, which origi-

nates from the measurement technique.

The polynomial model generally shows very small uncertainties in its inference results, compared to the other models. Especially in the first few meters of the depth profile, but also in the intermediate depths, the confidence intervals are narrower than in other models. Although the models were trained on the same amount of simulations (except for the independent step model) the models differ in their confidence with which they infer observations. This effect originates from the way the depth profiles are represented in the prior distribution. The depth profile is represented via a combination of Legendre Polynomials and requires only five parameters to represent a depth profile. Training the conditional density estimators on a prior distribution with small amount of parameters seems to be beneficial in terms of uncertainty. However, the small uncertainties might be accountable for a prior distribution that is too restrictive. As already mentioned in section 3.3, the parameters are restricted such that the resulting polynomial is within the interval [-1,1] under which Legendre Polynomials are well-defined. This might be too restrictive and a potential reason for insufficient variability in the samples. This parameter restriction and the lack of sample variability might be accountable that the model is too confident in its predictions.

The depth profile of the block prior can be represented via seven parameters, related to layer resistivities and thicknesses (see section 2.2.3). Despite a similarly small number of parameters than the polynomial prior, it has greater uncertainties than the polynomial model. This is due to the fact that the block model is capable of inferring the maximal depth along with the resistivity values of the layers. As the results have demonstrated, there are many plausible depth profiles that match the observation equally well. Inference of depth along with layer resistivities increases the space of possible depth profiles, that fit to the same the observation. This uncertainty is partly related to the non-uniqueness of the forward model, which is even stronger represented when the depth is able to vary. At the same time, the simulation space is larger compared to the step model, which requires more simulation to cover this space. Therefore, the uncertainties might also be attributed to insufficient training. This contribution to the uncertainties can be solved easily through more simulations, however the uncertainty related to the non-uniqueness of the forward model cannot be solved.

The step model assumes a fixed depth of 24m, which is equal to that of the polynomial and the independent step model. However, as it infers the direct resistivity values of each layer, the depth profile consists of 48 parameters. Due to the large parameter space, the uncertainties are also larger than in the

polynomial model. As individual intermediate layers only have a small effect on the final apparent resistivity signal and might be superimposed by adjacent layers, it is difficult to accurately predict individual layers resistivities. To emphasize once more, the non-uniqueness of the forward model allows for multiple combinations of layer resistivities that produce the same signal. Individual layers are therefore hard to accurately determine, as their individual influence on the apparent resistivity can be equalized by other layers, which induces uncertainty into the model's predictions.

The independent step model has the same parametrization as the step model but is not constrained in its layer transitions by the resistivity values of previous layers. This leads to a much greater parameter space and induces a lot of uncertainty in the model. The independent step model shows the largest uncertainties across all models, despite being trained with five times more simulations than other models. To reduce the uncertainty, either a significantly greater number of simulations is required or a restriction of the parameter space of the prior distribution is necessary.

As discussed in this section, the uncertainty of models is strongly influenced by the parametrization of the prior distribution. This underlines the importance of choosing a suitable parameterization of the depth profile. Selecting an appropriate prior distribution is also dependent on other factors, as discussed in the next section.

4.2 Choice of Prior Distribution

Different characteristics of the subsurface structure were incorporated into the four models via the prior distributions. These characteristics are clearly present in the inferred posterior distributions, as the results strongly reflect the underlying prior on which they were trained (Fig. 3.1). This is a key advantage over classical inversion methods, as it enables incorporation of additional knowledge and characteristics into the inversion process and cannot be done in classical deterministic inversion frameworks. However, along with the choice of prior, bias and limitations are incorporated into the model. This raises the question, what is an adequate (or the best) prior distribution to represent the subsurface and its layer transitions, with respect to computational feasibility?

For the two step models, I used a fixed number of parameters, each of which represent a resistivity value of small discrete layers. The depth profile of the polynomial model is represented via the polynomials, but then evaluated within small steps that correspond to the same number of fixed-sized layers as in the step models. This limits the maximal depth of inversion achievable with

those models, due to the dependence on the prior parametrization. Ideally, the depth should be variable and must be inferred for each observation along with the depth profile. However, increasing the parameter space, to allow inference for greater depths, can lower inference accuracy or requires more simulations. This effect has been observed in the comparison of the regularized step model against the unconstrained independent step model. The block model is capable of inferring depth, which seems to be beneficial, as it is a robust and accurate inference model for many test instances. Inference of depth increases the flexibility of the model, as it allows for more versatile resistivity depth distributions. Despite increasing the simulation space that needs to be covered, inference of depth is a desired property when choosing a prior distribution.

Another limitation regarding the prior is the current assumption of resistivity values. Currently, depth profiles with resistivity values between 1 and 1,000 Ωm are simulated. For this exploratory work, this was a reasonable choice given the trade-off between a more generalized model and a larger parameter space, that would require excessively more simulations. To enable the models of inverting a broader range of resistivity values and soil types, this limitation needs to be resolved. One way to address this problem is brute-force, by increasing the maximum resistivity range and thereby increasing the prior space. To maintain the accuracy of the inference results, the artificial neural network needs to be trained on a sufficient amount of data to cover the increased prior space, which requires higher simulation costs.

With the step and the polynomial model, I was able to incorporate continuous transitions in the depth profiles. For transitions that actually are continuous, these models also perform best, but are not well suited for capturing discrete layer boundaries. Aiming for universal prior distributions that are able to represent both types of soil transitions, jumping random walks ([Tzevelekas and Stavrakakis, 2009](#)), could be employed. They support smooth transitions but also allow for large changes in resistivity for discrete layer boundaries. The work of [Zhao and Curtis \(2024\)](#) on "Variational Prior Replacement in Bayesian Inference and Inversion" could also be a field to address the topic, where they state that the prior information of a posterior distribution can be replaced by a new prior distribution. The choice of a versatile representation of the depth profile via the prior distribution remains to be a subject for further research, where this study provides a good foundation on which future work can be carried out.

The two smooth posteriors (step model and polynomial model) are very different in terms of computation and training costs. As briefly mentioned in the previous section, training the posterior network is strongly dependent on

the parametrization of the prior distribution. The polynomial prior is more simulation-efficient, as the parameter space is smaller. However, learning the parametrization is much harder in this context, as the likelihood of the individual parameters is very nonlinear. This dependency of the parameters is more complex, but therefore only a small amount of parameter distributions needs to be learned. The step prior distribution on the other hand has more parameters, but the likelihood of the individual parameters is relatively simple, as they directly represent the resistivity value of the layers. The same accounts for the independent step prior, however the large parameter space requires a larger amount of simulations to properly learn the relation of the parameters. The block prior again has smaller amount of parameters, but their individual likelihood is more complex, as it allows variation in depth. This relation increases the complexity of the likelihood of the parameters, as the resistivity values correspond to different locations in the depth profile, dependent on the parameters of the layer thickness. The likelihood is therefore harder to learn than in the step prior, but is coped by the small amount of parameters.

Considering the performance of the models, it seems beneficial to have a small number of parameters in the prior distribution. A prior of varying depth is more complex to learn but leads to more degrees of freedom and a more flexible and robust inference model. Incorporating smoothness into the prior leads to good inference results on smooth and non-smooth test instances, and is therefore a desired property. The aspects identified here should be considered when choosing a prior distribution for further probabilistic models that follow this work.

4.3 Evaluation and Limitations of Models Performance

There is one additional limitation to this approach that is not related to the prior distribution, but to the parametrization of the simulator. The conditional density estimator is trained on simulations that originate from the simulator, and therefore dependent on its parametrization. This means that the models are only able to infer new observations that correspond to the parameters, such as the electrode distances, as implemented in the simulator. Measurements that deviate from the implemented electrode distances (see 2.1) or have missing data cannot be inferred correctly. Especially for the applicability of the models on the web interface, this is a limiting factor and should be addressed, so that the models can be used across institutes or companies that use different surveying setups. The work of [Gloeckler et al. \(2024\)](#), on the new SBI variant "All-in-one simulation-based inference", addresses the limitation

of current SBI methods on the fixed parametrization of the simulator. This method is able to handle parametric and non-parametric simulators, which would eliminate the restriction of the fixed parametrization of electrode distances. Furthermore, All-in-one simulation-based inference is capable of handling unstructured and missing data. Especially the aspect of missing data is important, as real observations differ from simulations. Due to many reasons, it might not be feasible to always measure the same number of electrode distances for a given site. Requiring complete measurements under the pre-determined AB distances limits the applicability of the models to only those measurements. Removing this current constraint from missing values by employing All-in-one simulation-based inference, improves the applicability of the models. Addressing this current limitation with this new SBI variant is very promising and should be considered as a follow-up work on this project.

Despite the aforementioned limitations and the potential to improve this workflow, I was able to demonstrate that a probabilistic approach to inversion of VES is feasible. Also, the probabilistic models are able to outperform state-of-the-art deterministic inversion methods. The models' performance depend on the prior distribution on which the posteriors are trained and tested on. However, there is always a prior distribution and a probabilistic model that is able to outperform the deterministic ones. The smooth models (polynomial model and step model) perform well on test instances that represent a smooth depth profile, but also on test instances of distinct layer boundaries and abrupt transitions. Also, the block model is capable of inferring apparent resistivities of smooth and non-smooth soil profiles. This shows that the models have great applicability and are generally capable of inferring observations even outside the soil representation on which they were trained on. Future models that combine multiple features from our four prior distributions have the potential to provide robust inference under all test instances within one model, and might outperform the current probabilistic models. In terms of computational performance, the probabilistic models outperform the deterministic due to the amortization of the simulations costs. Deterministic inference requires computational effort on every new observation, whereas our models provide posterior samples nearly instantaneous.

Chapter 5

WebApplication - VESBI

Until now, there is no centralized or standardized way to perform inversion in geoelectric and geophysics in general. However, inversion is a widespread problem in many geophysical applications. Open source software tools for inversion such as pyGIMLi (Rücker et al., 2017) or SimPEG (Cockett et al., 2015) are available, but their use requires large commitment on the user side. The challenges of using these libraries begin with the installation of large packages, and a correct implementation of the forward model and inversion process. This requires a certain amount of time and commitment to get familiar with the programs and access to sufficient computing power to perform the inversion locally. Therefore, this type of inversion is hardly accessible to people, who do not have a certain level of programming skills. The individual setup of local inversion tools is also the reason for a lack of standard in this field, as hyperparameters of the inversion are always selected individually. With the

The same applies to the use of SBI. It is an open source library that can be used by everyone, but it requires time, effort, resources and certain amount of skills and knowledge to run the models locally. To minimize the hurdles of applicability for this method and inversion of VES in general, I decided to build a web application that employs the trained models. This platform highlights the benefits of the SBI method and is able to take full advantage of them.

With the essential advantage of amortization that is inherent to many SBI variants, the models are very well suited for fast evaluation within a real-time web-application. Results can be obtained nearly instantaneous, as no further simulations or training is required to evaluate new observations. This opens the possibility to directly evaluate measurements in the field via this platform. This probabilistic inversion method, allows providing uncertainties to the inference results, which is a second key advantage over deterministic methods. Fast evaluation in the field along with uncertainties have the potential

to improve the surveying process as well. Uncertainties can provide insight into how additional measurements could reduce uncertainty and identify areas where measurements are lacking. For instance, when facing significant uncertainty at specific depths or at the simulated apparent resistivities at corresponding AB/2 distances, additional measurements at intermediate AB/2 distances could reduce this uncertainty. Obtaining this immediate feedback in the field can be highly beneficial, as it can enhance both the quality of the measurements and the overall inference results.

Additionally, this platform has the potential to establish a certain standard for inversion procedures. As previously mentioned, conventional inversion techniques are lacking such a standard and depend on the individual setup of the inversion tools. Inversions made via this platform are derived from the same underlying neural networks, which sets a certain standard and therefore increases the comparability of results in this field.

At the same time, such an application offers a centralized platform for inversion. It is my hope that, in addition to the current trained models, more models that follow the presented workflow will be deployed on the platform. In this scenario, the web application has the potential to become a centralized tool for probabilistic inversion across geophysical disciplines.

5.1 Implementation Details

I build a user based platform that requires a minimal registration with an email address, password and optional personal data. In the first step of the inversion process, a file containing the measurement data is uploaded and additional information about the measurement can be linked to it. The supported file formats for uploading are .xls, .xlsx and .csv files. After a file has been uploaded (see Fig. 5.1 for a schematic workflow), the data is validated on the survey configuration and the measured data is processed. In the second stage of the inversion process, the user can select the model under which the inversion should run. The respective network is evaluated on the previously uploaded observation and derives the posterior distribution. The posterior samples are then evaluated under the forward model to provide poster predictive samples as well as the inferred depth profile. Finally, a plot is generated and send to the user containing inversion results along with uncertainties (Fig. 5.2).

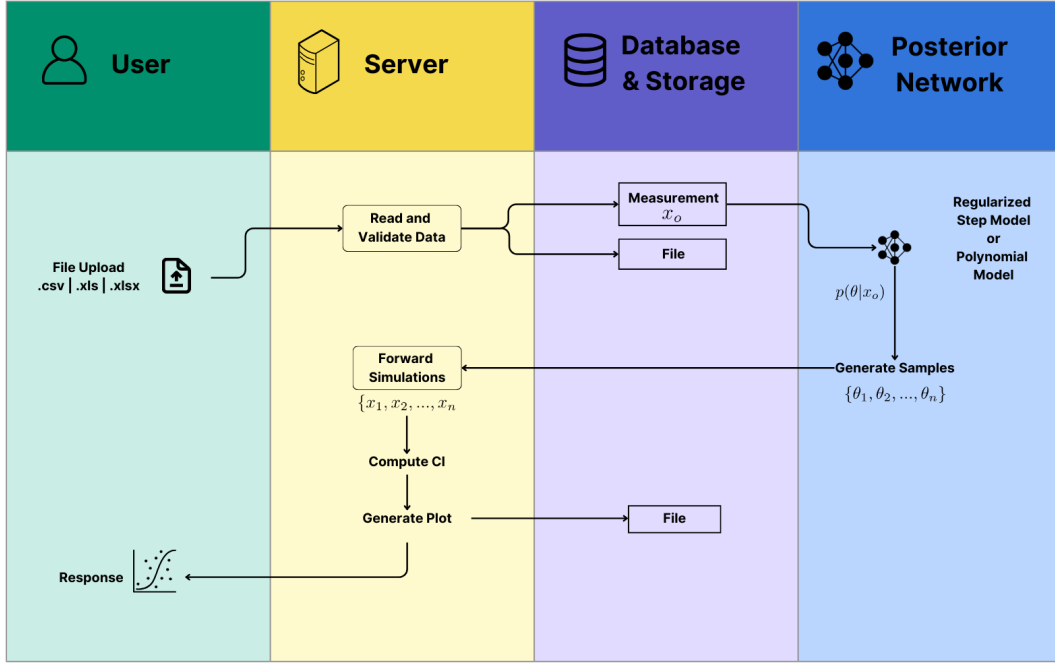


Figure 5.1: Workflow of the Inversion process in the VESBI Application. Illustration of the required steps from the file upload via the user to the final plot of the inference results. The process is divided into four parts, namely **User side** (Frontend) **Server** and **Database and Storage** (Backend) and the **Posterior Network**. Rectangles represent a backend entity, that is saved in the database. File entities are also stored in the local storage service.

5.2 Outlook on additional Features

This platform is in an early stage of development and is not yet fully mature. Given the timeframe of six months of a master thesis, it was not feasible to build a holistic and fully developed web application, in addition to implementing and validating the models. Hence, this platform was a first exploration of this area. A workflow with basic functionality has been implemented, which evaluates the underlying networks on uploaded measurements and returns corresponding inference results. In order to fully realize the potential of this platform and transform it into a fully mature application, additional features need to be implemented. As a first step, I would address the restriction that allows only the inversion of measurements that follow our specific electrode spacing. Removing this limitation (for example, by employing the SBI Simformer variant (Gloeckler et al., 2024)), would significantly enhance the platform's applicability. The same accounts for the limitations that are inherent to the current prior distributions, such as the fixed depth of inversion or the limitation to supported resistivity ranges.

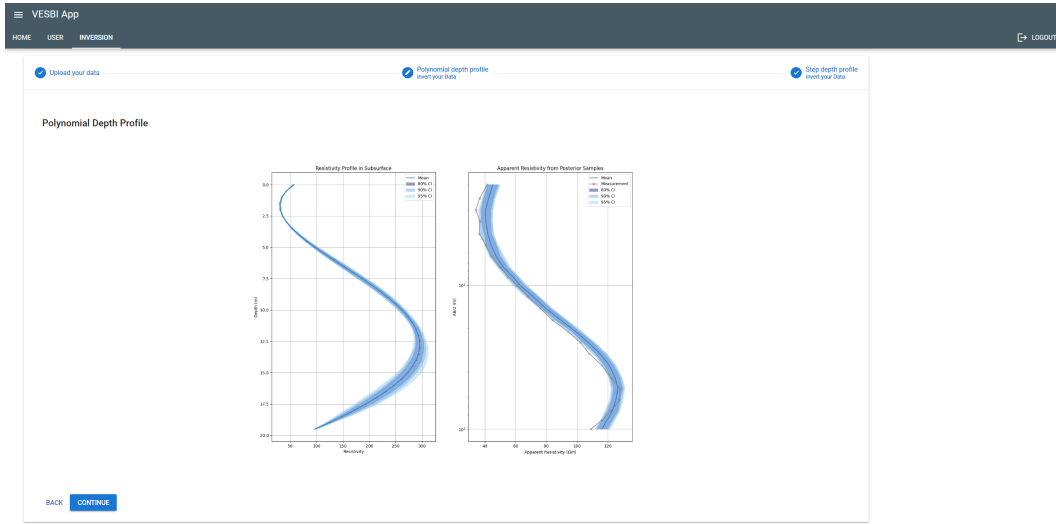


Figure 5.2: Screenshot of web application after successful inversion of a VES under the polynomial model. The inferred depth profile is shown on the left plot, with different confidence intervals. The posterior predictive samples and their uncertainty on the right plot.

Currently, only single observations can be uploaded and evaluated at once. In terms of usability, I suggest implementing an upload of multiple measurements at once and provide a user history of previous inversions. These two features, are technically related and could be implemented simultaneously. They allow a much easier and more versatile workflow for inverting results. In addition to the multi measurement upload, I would also incorporate e-mail notification such that a user is able to upload multiple measurements at once and receives a notification when all measurements are inverted.

As a long term goal, it would be highly beneficial to develop real time inversion with our models, that is capable of inverting the preliminary measurements. This enables direct evaluation while measuring in the field. Such a direct response indicating the inferred depth reached via the current AB/2 spacings along with the uncertainties are super valuable information when surveying, which cannot be done with current inversion tools.

Chapter 6

Conclusion

Vertical electrical sounding (VES) is an important method in the field of geoelectrics and is commonly used to image the Earth's subsurface. To derive the resistivity depth profile of the subsurface, the observations of VES require inversion, which until now is conducted in a non-standardized manner. Current inversion methods have shortcomings and limitations such as their assumption of number of existing layers prior to inversion, the lack of uncertainty quantification, and their determinism.

Within this work, I initiated a probabilistic approach towards inversion of VES, using simulation-based inference (SBI) to overcome the limitations of deterministic inversion methods. I demonstrated the feasibility of this approach and its potential to address the shortcomings of traditional VES inversion. This approach holds great promise for improving inversion in the field of geoelectrics by providing uncertainty quantification, but also in terms of accuracy and performance.

The four probabilistic models were able to outperform the deterministic models in terms of minimal root mean square error (RMSE) of the posterior predictive samples, with at least one probabilistic model achieving higher accuracy than any of the deterministic models across all test instances. Furthermore, the probabilistic models (except for the independent step model) outperform those deterministic models with the same number of layers in nearly all test instances. The 48-layer step model yields lower errors than the 48-layer deterministic model in three out of four test instances, and on average across all instances. The probabilistic four-layer model is also capable to yield more accurate results than the four-layer deterministic model in three out of four instances and also on average.

With the variety of depth profiles that fit the observations equally well, I

was able to demonstrate the degeneracy of the forward model. Given the non-uniqueness of the forward model, it seems insufficient to provide only a single “best-fitting” result, as in the case of deterministic models. This validates the probabilistic approach taken in this study, and emphasizes the importance of providing uncertainties to the inference results.

However, the performance of the probabilistic models depend on the test instances and on the prior distribution on which they were trained. Due to the prior distribution, soil characteristics could be incorporated into the inference process, which are clearly represented in the posterior distributions. It is not straightforward to integrate such features into the inference process of deterministic models. However, the prior distribution is also the source of some of the limitations of the models, such as the range of resistivity values, or the maximal depth that can be inferred. I was able to identify important aspects for the choice of a suitable prior distribution on future probabilistic models. It is desired to define a distribution with few parameters that is able to infer depth and incorporates smoothness as well as abrupt resistivity transitions in its depth profiles. Jumping random walks is a possible prior distribution that combines some of these desired features. However, the selection of an appropriate prior distribution remains a topic for future research that can be built on this work.

With the goal to strive towards greater uniformity in the inversion process, I laid the groundwork for a web based application for inversion of VES. Due to the scope of this thesis, I had to limit certain features of this web application. However, I was able to implement a web-based inversion tool employing pre-trained neural networks. The application has shown the potential to provide a centralized and user-friendly tool for inversion, without the need for individual installation or implementation of software. Once the limitations of the platform as highlighted in this thesis are overcome, this platform enables a fast, centralized, and standardized way towards VES inversion.

In this work, I was able to address multiple shortcomings of classical deterministic inversion of VES. The models showed the capacity to meet and even outperform current state-of-the-art inversion methods. Ultimately, I was able to initialize a platform for standardized and centralized inversion in the geoelectric domain. I hope that this workflow will be applied to other geophysical inversion problems and that this platform will host further inversion models in the future.

Acknowledgments

I want to thank Prof. Dr. Jakob Macke and Prof. Dr. Reinhard Drews, who gave me the possibility to combine my interests in geoscience and machine learning within this master thesis. I want to thank Reinhard Drews, in particular, who gave me interesting ideas and good feedback in the course of my thesis. At the same time, he gave me the possibility to decide on the further direction of the project, for which I am very grateful.

I would like to give a special thanks to Guy Moss. You always gave me time to ask questions and gave me new ideas on current problems and further directions of this project. I am honestly impressed by how fast you are able to understand problems and directly have multiple solutions to them in mind. I want to thank you for your guidance within this thesis, your valuable feedback and your excellent supervision in general. I also want to thank Rebecca Schlegel who took the time to read my thesis and provided many of good comments, which helped me a lot. Also, your encouragement and support during my thesis was invaluable. In general, I want to thank the Geophysics group for their hospitality and the interesting discussions we had during lunchtime and coffee breaks.

I want to acknowledge support by the state of Baden-Württemberg through bwHPC, to grant me access to the cluster on which the main part of the project was executed. I would also like to thank Terrana Geophysics for taking the time to go through their archives with me and providing me data for my work.

Bibliography

- Abdullahi, M. (2015). The Application of Vertical Electrical Sounding (VES) for Groundwater Exploration in Tudun Wada Kano State, Nigeria. *Journal of Geology & Geosciences*, 04.
- Appel, E., Wilhelm, J., and Waldhör, M. (1997). Archaeological prospection of wall remains using geoelectrical methods and GPR. *Archaeological Prospection*, 4(4):219–229.
- Best, M. E. (2015). 11.15 - Mineral Resources. In Schubert, G., editor, *Treatise on Geophysics (Second Edition)*, pages 525–556. Elsevier, Oxford.
- Binley, A. and Slater, L. (2020a). Electrical Properties of the Near-Surface Earth. In Binley, A. and Slater, L., editors, *Resistivity and Induced Polarization: Theory and Applications to the Near-Surface Earth*, pages 18–99. Cambridge University Press, Cambridge.
- Binley, A. and Slater, L. (2020b). Field-Scale Data Acquisition. In Binley, A. and Slater, L., editors, *Resistivity and Induced Polarization: Theory and Applications to the Near-Surface Earth*, pages 154–212. Cambridge University Press, Cambridge.
- Bishop, C. M. (1995). Training with Noise is Equivalent to Tikhonov Regularization. *Neural Computation*, 7(1):108–116.
- Blatter, D., Morzfeld, M., Key, K., and Constable, S. (2022). Uncertainty quantification for regularized inversion of electromagnetic geophysical data – Part II: application in 1-D and 2-D problems. *Geophysical Journal International*, 231(2):1075–1095.
- Bortolozo, C. A., Porsani, J. L., Santos, F. A. M. d., and Almeida, E. R. (2015). VES/TEM 1D joint inversion by using Controlled Random Search (CRS) algorithm. *Journal of Applied Geophysics*, 112:157–174.
- Chambers, J. E., Kuras, O., Meldrum, P. I., Ogilvy, R. D., and Hollands, J. (2006). Electrical resistivity tomography applied to geologic, hydrogeologic, and engineering investigations at a former waste-disposal site. *Geophysics*, 71(6):B231–B239.

- Cockett, R., Kang, S., Heagy, L. J., Pidlisecky, A., and Oldenburg, D. W. (2015). Simpeg: An open source framework for simulation and gradient based parameter estimation in geophysical applications. *Computers & Geosciences*.
- Cranmer, K., Brehmer, J., and Louppe, G. (2020). The frontier of simulation-based inference. *Proceedings of the National Academy of Sciences*, 117(48):30055–30062.
- Dalmasso, N., Pospisil, T., Lee, A. B., Izbicki, R., Freeman, P. E., and Malz, A. I. (2020). Conditional Density Estimation Tools in Python and R with Applications to Photometric Redshifts and Likelihood-Free Cosmological Inference. *Astronomy and Computing*, 30:100362.
- Deistler, M., Goncalves, P. J., and Macke, J. H. (2022). Truncated proposals for scalable and hassle-free simulation-based inference.
- Durkan, C., Bekasov, A., Murray, I., and Papamakarios, G. (2019). Neural Spline Flows.
- El Makrini, S., Boualoul, M., Mamouch, Y., El Makrini, H., Allaoui, A., Randazzo, G., Roubil, A., El Hafyani, M., Lanza, S., and Muzirafuti, A. (2022). Vertical electrical sounding (ves) technique to map potential aquifers of the guigou plain (middle atlas, morocco): Hydrogeological implications. *Applied Sciences*, 12(24).
- El-Qady, G. and Ushijima, K. (2001). Inversion of DC resistivity data using neural networks. *Geophysical Prospecting*, 49(4):417–430.
- Gloeckler, M., Deistler, M., Weilbach, C., Wood, F., and Macke, J. H. (2024). All-in-one simulation-based inference.
- Graves, A., Mohamed, A.-r., and Hinton, G. (2013). Speech recognition with deep recurrent neural networks. In *2013 IEEE International Conference on Acoustics, Speech and Signal Processing*, pages 6645–6649.
- Greenberg, D. S., Nonnenmacher, M., and Macke, J. H. (2019). Automatic Posterior Transformation for Likelihood-Free Inference.
- Heriyanto, M. and Srigutomo, W. (2017). 1-D DC Resistivity Inversion Using Singular Value Decomposition and Levenberg-Marquardt’s Inversion Schemes. *Journal of Physics: Conference Series*, 877:012066.
- Hermans, J., Banik, N., Weniger, C., Bertone, G., and Louppe, G. (2021). Towards constraining warm dark matter with stellar streams through neural simulation-based inference. *Monthly Notices of the Royal Astronomical Society*, 507(2):1999–2011.

- Hermans, J., Delaunoy, A., Rozet, F., Wehenkel, A., Begy, V., and Louppe, G. (2022). A Trust Crisis In Simulation-Based Inference? Your Posterior Approximations Can Be Unfaithful.
- Hoversten, G. M., Dey, A., and Morrison, H. F. (1982). Comparison of Five Least-Squares Inversion Techniques in Resistivity Sounding*. *Geophysical Prospecting*, 30(5):688–715.
- Inman, J. R. (1975). Resistivity inversion with ridge regression. *GEO-PHYSICS*, 40(5):798–817.
- Inman, J. R., Ryu, J., and Ward, S. H. (1973). Resistivity inversion. *Geophysics*, 38(6):1088–1108.
- Koganti, T., Van De Vijver, E., Allred, B. J., Greve, M. H., Ringgaard, J., and Iversen, B. V. (2020). Mapping of Agricultural Subsurface Drainage Systems Using a Frequency-Domain Ground Penetrating Radar and Evaluating Its Performance Using a Single-Frequency Multi-Receiver Electromagnetic Induction Instrument. *Sensors*, 20(14):3922.
- Linderholm, P., Marescot, L., Loke, M. H., and Renaud, P. (2008). Cell culture imaging using microimpedance tomography. *IEEE transactions on biomedical engineering*, 55(1):138–146.
- Lines, L. and Treitel, S. (1984). A Review of Least-Squares Inversion and Its Application to Geophysical Problems*. *Geophysical Prospecting*, 32(2):159–186.
- Loke, M. H., Chambers, J. E., Rucker, D. F., Kuras, O., and Wilkinson, P. B. (2013). Recent developments in the direct-current geoelectrical imaging method. *Journal of Applied Geophysics*, 95:135–156.
- Lopez-Gomez, I., Christopoulos, C., Langeland Ervik, H. L., Dunbar, O. R. A., Cohen, Y., and Schneider, T. (2022). Training Physics-Based Machine-Learning Parameterizations With Gradient-Free Ensemble Kalman Methods. *Journal of Advances in Modeling Earth Systems*, 14(8):e2022MS003105.
- McCarthy, J. and Zachara, J. (1989). ES&T Features: Subsurface transport of contaminants. *Environmental Science & Technology*, 23(5):496–502.
- McGillivray, P. R. (1992). FORWARD MODELING AND INVERSION OF DC RESISTIVITY AND MMR DATA.
- Miller, B. K., Cole, A., Forré, P., Louppe, G., and Weniger, C. (2021). Truncated Marginal Neural Ratio Estimation.

- Moss, G., Višnjević, V., Eisen, O., Oraschewski, F. M., Schröder, C., Macke, J. H., and Drews, R. (2023). Simulation-Based Inference of Surface Accumulation and Basal Melt Rates of an Antarctic Ice Shelf from Isochronal Layers.
- Papamakarios, G. and Murray, I. (2018). Fast $\$\\epsilon$ -free Inference of Simulation Models with Bayesian Conditional Density Estimation.
- Piatti, C., Boiero, D., Godio, A., and Socco, L. V. (2010). Improved Monte Carlo 1D inversion of vertical electrical sounding and time-domain electromagnetic data. *Near Surface Geophysics*, 8(2):117–133.
- Pétron, G., Granier, C., Khattatov, B., Lamarque, J.-F., Yudin, V., Müller, J.-F., and Gille, J. (2002). Inverse modeling of carbon monoxide surface emissions using Climate Monitoring and Diagnostics Laboratory network observations. *Journal of Geophysical Research: Atmospheres*, 107(D24):ACH 10–1–ACH 10–23.
- Reed, R. and Marks, R. J. (1999). *Neural Smithing: Supervised Learning in Feedforward Artificial Neural Networks*. The MIT Press.
- Reynolds, J. (2011). An Introduction to Applied and Environmental Geophysics.
- Riss, J., Luis Fernández-Martínez, J., Sirieix, C., Harmouzi, O., Marache, A., and Essahlaoui, A. (2011). A methodology for converting traditional vertical electrical soundings into 2D resistivity models: Application to the Saïss basin, Morocco. *Geophysics*, 76(6):B225–B236.
- Roemmich, D. (1981). Circulation of the Caribbean Sea: A well-resolved inverse problem. *Journal of Geophysical Research: Oceans*, 86(C9):7993–8005.
- Rozet, F. and Fin, U. d. L. > M. i. c. s. d. (2021). Arbitrary Marginal Neural Ratio Estimation for Likelihood-free Inference.
- Rücker, C., Günther, T., and Wagner, F. M. (2017). pyGIMLi: An open-source library for modelling and inversion in geophysics. *Computers and Geosciences*, 109:106–123.
- Russell, B. and Hampson, D. (1991). Comparison of poststack seismic inversion methods. In *SEG Technical Program Expanded Abstracts 1991*, SEG Technical Program Expanded Abstracts, pages 876–878. Society of Exploration Geophysicists.
- Seidel, K. and Lange, G. (2007). *Direct Current Resistivity Methods*, pages 205–237. Springer Berlin Heidelberg, Berlin, Heidelberg.

- Shorten, C. and Khoshgoftaar, T. M. (2019). A survey on Image Data Augmentation for Deep Learning. *Journal of Big Data*, 6(1):60.
- Snieder, R. and Trampert, J. (1999). Inverse Problems in Geophysics. In Wirgin, A., editor, *Wavefield Inversion*, pages 119–190, Vienna. Springer.
- Stephen, J., Manoj, C., and Singh, S. B. (2004). A direct inversion scheme for deep resistivity sounding data using artificial neural networks. *Journal of Earth System Science*, 113(1):49–66.
- Storz and Jacobs, F. (2001). Electrical resistivity tomography to investigate geological structures of the earth’s upper crust. *Geophysical Prospecting*, 48:455–471.
- Tejero-Cantero, A., Boelts, J., Deistler, M., Lueckmann, J.-M., Durkan, C., Gonçalves, P. J., Greenberg, D. S., and Macke, J. H. (2020). sbi: A toolkit for simulation-based inference. *Journal of Open Source Software*, 5(52):2505.
- Tobler, W. R. (1970). A Computer Movie Simulating Urban Growth in the Detroit Region. *Economic Geography*, 46:234–240.
- Tzevelekas, L. and Stavrakakis, I. (2009). Improving partial cover of Random Walks in large-scale Wireless Sensor Networks. In *2009 IEEE International Symposium on a World of Wireless, Mobile and Multimedia Networks & Workshops*, pages 1–6.
- Van Ree, C. C. D. F. and van Beukering, P. J. H. (2016). Geosystem services: A concept in support of sustainable development of the subsurface. *Ecosystem Services*, 20:30–36.
- Volchko, Y., Norrman, J., Ericsson, L. O., Nilsson, K. L., Markstedt, A., Öberg, M., Mossmark, F., Bobylev, N., and Tengborg, P. (2020). Subsurface planning: Towards a common understanding of the subsurface as a multifunctional resource. *Land Use Policy*, 90:104316.
- Zarroca, M., Bach, J., Linares, R., and Pellicer, X. M. (2011). Electrical methods (VES and ERT) for identifying, mapping and monitoring different saline domains in a coastal plain region (Alt Empordà, Northern Spain). *Journal of Hydrology*, 409(1):407–422.
- Zhao, X. and Curtis, A. (2024). Variational Prior Replacement in Bayesian Inference and Inversion.
- Zhou, H., Gómez-Hernández, J. J., and Li, L. (2014). Inverse methods in hydrogeology: Evolution and recent trends. *Advances in Water Resources*, 63:22–37.

Appendix

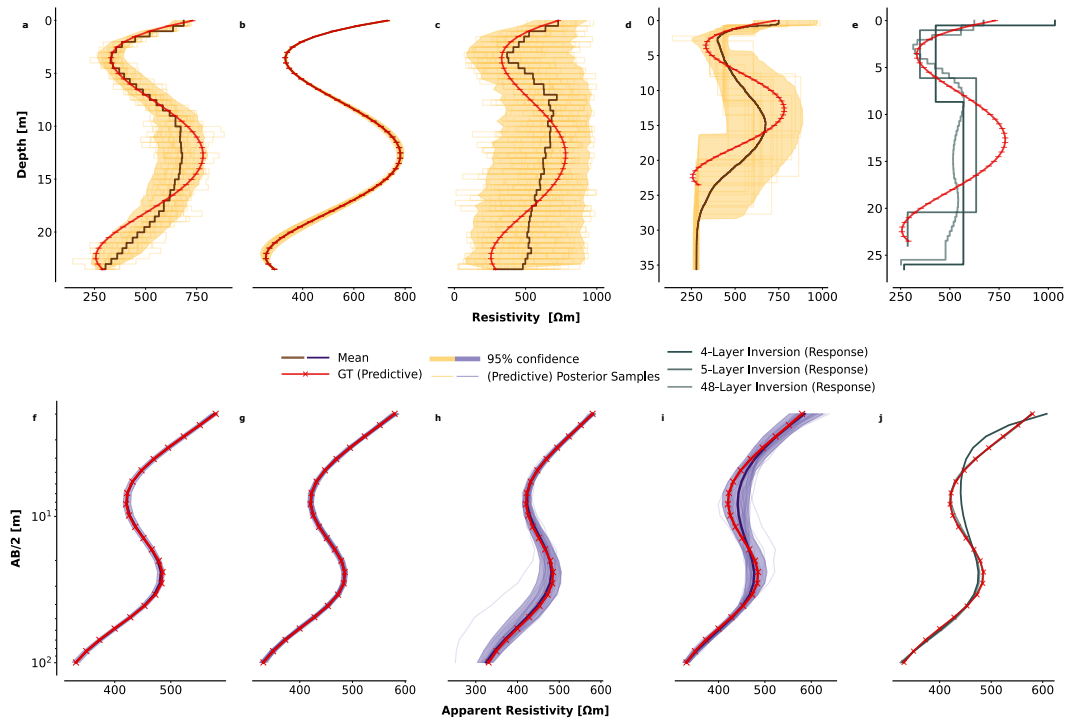


Figure 6.1: Posterior (Predictive) for synthetic ground truth from Legendre polynomial prior. Subplots a - e show the depth resistivity profile in parameter space, f-j show apparent resistivity against AB electrode spacing in observation space. Solid lines are the posterior mean, the shaded areas are 5th and 95th percentiles. Light colored are individual posterior (predictive) samples. a shows the model posterior network trained on the independent step prior, b on polynomial prior, c on independent step prior d on block prior. The respective posterior predictive of the models are showcased below. e and j show inversion and response of classic deterministic inversion of four, five and 48-layers.

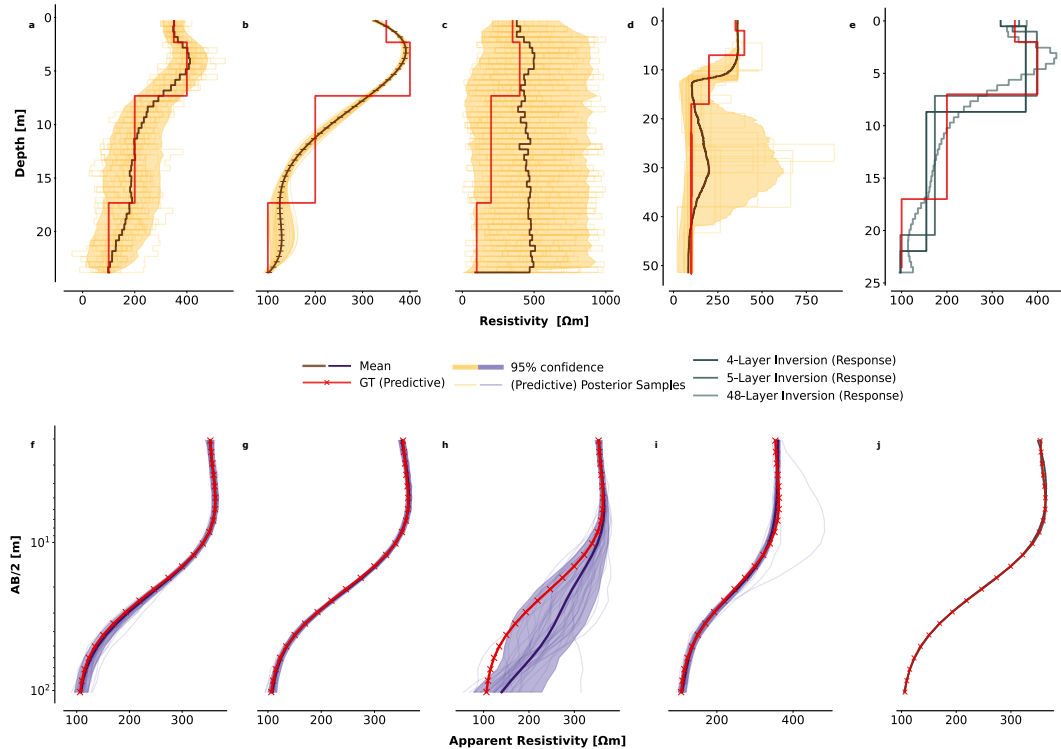


Figure 6.2: Posterior (Predictive) for synthetic ground truth from four-layer block prior. Subplots a - e show the depth resistivity profile in parameter space, f-j show apparent resistivity against AB electrode spacing in observation space. Solid lines are the posterior mean, the shaded areas are 5th and 95th percentiles. Light colored are individual posterior (predictive) samples. a shows the model posterior network trained on the independent step prior, b on polynomial prior, c on independent step prior d on block prior. The respective posterior predictive of the models are showcased below. e and j show inversion and response of classic deterministic inversion of four, five and 48-layers.

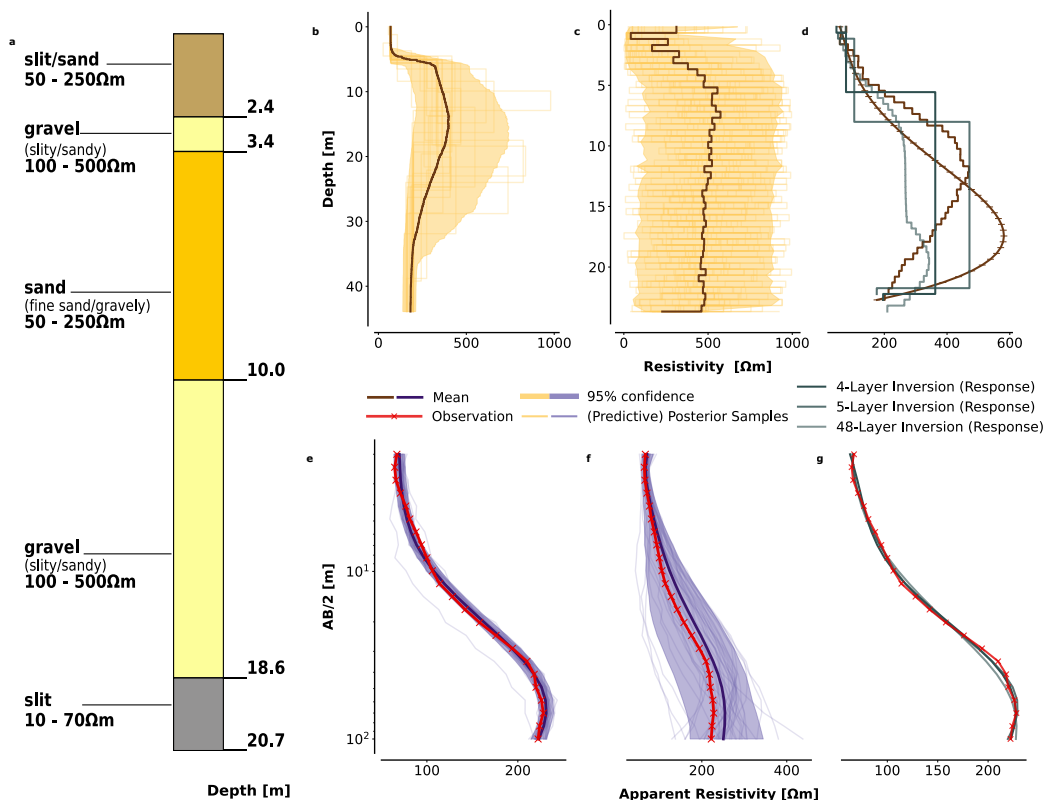


Figure 6.3: Inference results of step model and polynomial model on real VES data, that is confirmed by sediment core. Subplot a represents the sediment core that has been grouped into five layers by Terrana Geophysik. Subplot b and c show the posterior distribution of the block and independent step model. The posterior predictive distribution is shown below in e and f, d and f show the results of the deterministic inversion models.

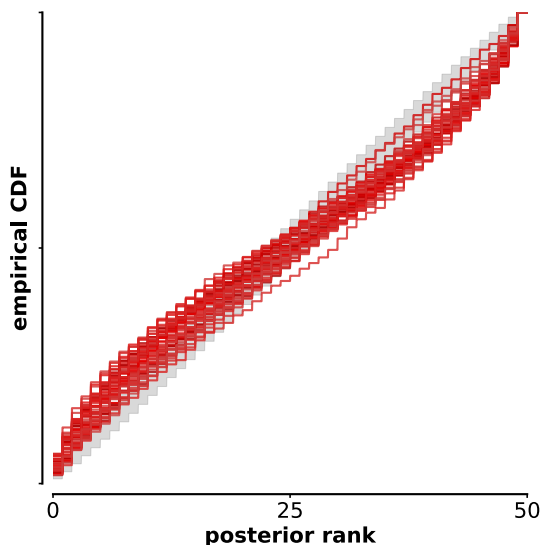


Figure 6.4: Simulation Based Calibration of posterior ranks from the independent step model. The gray shaded area represents the 95% confidence interval of a uniform distribution of ranks. The red lines are the cumulative density function for each of the 48 parameters. A well calibrated model lies within the support of the uniform distribution.